

Efficient Recovery of Sparse Graph Signals from Graph Filter Outputs

Gal Morgenstern *Student Member, IEEE*, and Tirza Routtenberg, *Senior Member, IEEE*

Abstract— This paper investigates the recovery of a node-domain sparse graph signal from the output of a graph filter. This problem, which is often referred to as the identification of the source of a diffused sparse graph signal, is seminal in the field of graph signal processing (GSP). Sparse graph signals can be used in the modeling of a variety of real-world applications in networks, such as social, biological, and power systems, and enable various GSP tasks, such as graph signal reconstruction, blind deconvolution, and sampling. In this paper, we assume double sparsity of both the graph signal and the graph topology, as well as a low-order graph filter. We propose three algorithms to reconstruct the support set of the input sparse graph signal from the graph filter output samples, leveraging these assumptions and the generalized information criterion (GIC). First, we describe the graph multiple GIC (GM-GIC) method, which is based on partitioning the dictionary elements (graph filter matrix columns) that capture information on the signal into smaller subsets. Then, the local GICs are computed for each subset and aggregated to make a global decision. Second, inspired by the well-known branch and bound (BNB) approach, we develop the graph-based branch and bound GIC (graph-BNB-GIC), and incorporate a new tractable heuristic bound tailored to the graph and graph filter characteristics. In addition, we propose the graph-based first order correction (GFOC) method, which improves existing sparse recovery methods by iteratively examining potential improvements to the GIC cost function by replacing elements from the estimated support set with elements from their one-hop neighborhood. Simulations on stochastic block model (SBM) graphs demonstrate that the proposed sparse recovery methods outperform existing techniques in terms of support set recovery and mean-squared-error (MSE), without significant computational overhead. In addition, we investigate the application of our graph-based sparse recovery methods in blind deconvolution scenarios where the graph filter is unknown. Simulations using real-world data from brain networks and pandemic diffusion analysis further demonstrate the superiority of our approach compared to graph blind deconvolution techniques.

Index Terms—Graph signal processing (GSP), support set recovery, double sparsity, generalized information criterion (GIC), graph signals, graph filters

I. INTRODUCTION

Graph signal processing (GSP) theory extends classical time-varying signals to irregular domains represented by graphs [2]–[4]. The graph under consideration may represent a physical network, such as electrical or sensor networks, or

a virtual network, such as social networks, or it may encode statistical dependencies among the signal values. Recent developments in GSP encompass a wide array of processing tools, including graph spectral analysis [5], [6], anomaly detection [7], sampling and signal recovery [8]–[14], verification of graph smoothness [15], [16], and graph filter design [2], [3], [17], [18]. However, limited attention has been paid to developing GSP-based techniques for the sparse recovery of node-domain *sparse graph signals*.

Signal modeling based on sparse representations is used in numerous signal and image processing applications [19]–[22]. Sparse recovery methods can broadly be categorized into three main groups: convex relaxations, often using methods such as ℓ_1 -norm minimization or basis pursuit [19], [23]–[26], non-convex optimization approaches [27]–[29], and greedy algorithms [20], [30]–[33]. In the context of estimation theory, Bayesian inference approaches estimate the sparse signal by incorporating prior information, while other methods use the structure of the dictionary matrix. In network science, compressed sensing and group testing have been discussed in [34]–[36], and diffusion processes that originate from a sparse signal have been discussed in [37]–[41]. Several GSP studies have investigated the sampling and reconstruction of graph signals by assuming the signal belongs to a vector subspace. For example, the works [42]–[45] assume graph bandlimited signals, while [46] considers sparsity in the spectral domain. Similarly, [47] models the graph signals as smooth in the node domain or decaying in the spectral domain.

Recently there has been growing interest in setups where a node-domain sparse graph signal \mathbf{x} is filtered by a graph filter \mathbf{H} . In this case, the output signal \mathbf{y} is referred to as a diffused sparse graph signal [48]. Modeling diffusion processes over graphs by graph filters is valuable due to the ability to capture local interactions among nodes [49]–[52]. Diffused sparse graph signals can be used for modeling many real-world network scenarios. For instance, in social networks, these signals can be used for opinion forming [53] and finding the origin of a rumor [54]. In biological networks, they enable the analysis of the spread of a disease [55], and in computer networks, they can be used to locate malware [56]. In power systems, they may be used for locating anomalies in power signals [57], [58]. In the field of GSP, diffused sparse graph signals have been studied in several problems, such as bandlimited graph signal reconstruction [59]. Blind deconvolution, in which both the graph filter and the sparse input are estimated, has been discussed in [48], [49], [60]–[62]. System identification, considered in [48], [50], refers to the case where the sparse signal is known, but the graph filter

G. Morgenstern and T. Routtenberg are with the School of ECE, Ben-Gurion University of the Negev, Beer Sheva, Israel (e-mail: {galmo@post.tirzar}@bgu.ac.il). This work is partially supported by the Israel Science Foundation (grant No. 1148/22), the Jabotinsky Scholarship from the Israel Ministry of Technology and Science, and the Israel Ministry of National Infrastructure and Energy. Parts of this work (the GM-GIC algorithm) were presented at the IEEE Computational Advances in Multi-Sensor Adaptive Processing (CAMSAP) Workshop 2023 [1].

coefficients are estimated. The sampling of diffused sparse graph signals is discussed in [63]. For an overview of blind deconvolution and signal reconstruction methods for diffused sparse graph signals, we refer the readers to Fig. 1 in [48]. However, in most of the applications discussed above, the sparse recovery does not exploit the GSP-based modeling of the *sparse graph signals*. Instead, these methods typically rely on standard sparse approximations, such as ℓ_1 relaxation, or employ tailored solutions that use specific properties of the application at hand.

In this paper, we establish efficient sparse recovery methods for graph signals using the generalized information criterion (GIC) [64] as the cost function. We assume double sparsity of both the graph and the graph signal and that the network diffusion process is modeled by a known low-degree graph filter. A direct solution for the GIC-based problem necessitates an exhaustive search, whose complexity grows exponentially with the size of the graph, rendering it impractical. We propose three graph-based sparse recovery methods that harvest the double sparsity imposed by the graph and the graph signal. The first method, the graph-based multiple GIC (GM-GIC) method, identifies and partitions a set of suspected nodes and then applies a local GIC on each partition, which significantly reduces the computational overhead of the GIC-based approach. The second method, the graph-based branch and bound GIC (Graph-BNB-GIC) method, further mitigates the computational demands by iteratively searching over the candidate support sets of the sparse graph signals (the same sets as in the GM-GIC method). This method is developed based on the branch and bound (BNB) method [65], [66] with a heuristic graph-based upper bound that exploits the double sparsity and the graph properties. The third method, the graph-based first order correction (GFOC) method, builds upon existing sparse recovery techniques and improves them in terms of the GIC cost function by replacing elements from the estimated support set with elements from their one-hop neighborhood. Our simulations on stochastic block model (SBM) graphs demonstrate that the proposed methods outperform state-of-the-art techniques: orthogonal matching pursuit (OMP), Lasso, and BNB with ℓ_1 regularization methods in terms of the support set recovery accuracy and mean squared error (MSE), without a significant computation overhead. In addition, to address scenarios where the graph filter is unknown, we introduce a new approach that incorporates a preliminary blind deconvolution stage to estimate the graph filter. Our simulations demonstrate that the proposed graph-based recovery methods can significantly improve the performance of existing graph blind deconvolution techniques in real-world applications, including: (1) brain networks obtained from real data [67]; and (2) the identification of the source of a disease using data from the 1854 cholera outbreak [68], [69].

The paper is organized as follows. Section II presents the necessary background and outlines the problem formulation. In Section III, we analyze the dictionary matrix for the proposed graphical setting. We describe both the GM-GIC and Graph-BNB-GIC methods in Section IV, followed by the presentation of the GFOC method in Section V. In Section VI, we present the simulation results, and the conclusions are

provided in Section VII.

Notations: In the rest of this paper, vectors and matrices are denoted by boldface lowercase and uppercase letters, respectively. The (k, m) th element of the matrix \mathbf{H} is denoted by $H_{k,m}$. The vector \mathbf{x}_Ω is a subvector of \mathbf{x} with the elements indexed by the set Ω , and \mathbf{H}_Ω is the submatrix of \mathbf{H} consisting of the *columns* indexed by Ω . In particular, \mathbf{H}_k denotes the k th column of \mathbf{H} . The projection matrix into the subspace $\text{col}(\mathbf{H}_\Omega)$ is given by

$$\mathbf{P}_{\mathbf{H}_\Omega} = \mathbf{H}_\Omega(\mathbf{H}_\Omega^T \mathbf{H}_\Omega)^{-1} \mathbf{H}_\Omega^T. \quad (1)$$

The operators $\|\cdot\|$, $\|\cdot\|_1$, $\|\cdot\|_0$, and $|\cdot|$ denote the Euclidean norm, ℓ_1 norm, zero semi-norm, and set cardinality. The identity matrix is denoted by \mathbf{I} .

II. PROBLEM FORMULATION

In this section, we formulate the problem of recovering a sparse graph signal from the outputs of a graph filter. First, in Subsection II-A, we present relevant GSP background. Then, in Subsection II-B, we outline the graphical setting considered. Finally, in Subsection II-C, we present the recovery problem addressed in this paper.

A. Background: Graphs and Graph Filters

Consider an undirected weighted graph $\mathcal{G}(\mathcal{V}, \mathcal{E})$, which consists of a set of nodes (vertices) \mathcal{V} , a set of edges \mathcal{E} , and a set of weights $\{w_e\}_{e \in \mathcal{E}}$. A graph signal is a mapping from the graph nodes into a $|\mathcal{V}| \times 1$ real vector:

$$\mathbf{x} : \mathcal{V} \rightarrow \mathbb{R}^{|\mathcal{V}|}. \quad (2)$$

A graph shift operator (GSO), $\mathbf{S} \in \mathbb{R}^{|\mathcal{V}| \times |\mathcal{V}|}$, is a linear operator applied on graph signals that satisfies

$$S_{k,m} = 0, \quad \text{if } \delta(k, m) > 1, \quad \forall k, m \in \mathcal{V}, \quad (3)$$

where the geodesic distance between nodes k and m , $\delta(k, m)$, is the number of edges on the shortest path between these nodes. According to (3), the non-zero elements of $\mathbf{S}_{k,m}$ are the diagonal elements (i.e. $k = m$) or the elements that are associated with an edge (i.e. $(k, m) \in \mathcal{E}$). As a result, by applying a GSO on a graph signal \mathbf{x} , each element of the shifted signal, $\mathbf{S}\mathbf{x}$, is a linear combination of the signal elements in its one-hop neighborhood:

$$[\mathbf{S}\mathbf{x}]_k = \sum_{m \in \mathcal{N}_1[k]} S_{k,m} x_m, \quad k = 1, \dots, |\mathcal{V}|, \quad (4)$$

where

$$\mathcal{N}_\Delta[k] = \{m \in \mathcal{V} : 0 \leq \delta(k, m) \leq \Delta\}, \quad \forall k \in \mathcal{V}. \quad (5)$$

Thus, the transformation by the GSO can be computed locally at each node by aggregating the values of the input signal within the one-hop neighborhood of each node.

A shift-invariant graph filter, $\mathbf{H} \in \mathbb{R}^{|\mathcal{V}| \times |\mathcal{V}|}$, is defined as a polynomial of the GSO [3], [4]:

$$\mathbf{H} = h_0 \mathbf{I} + h_1 \mathbf{S} + \dots + h_\Psi \mathbf{S}^\Psi, \quad (6)$$

where h_0, \dots, h_Ψ are the coefficients of the graph filter and $1 \leq \Psi \leq |\mathcal{V}| - 1$ is the graph filter order. By substituting (3) in (6) it can be verified that the (k, m) th element of \mathbf{H} satisfies

$$H_{k,m} = \sum_{i=0}^{\Psi} h_i [\mathbf{S}^i]_{k,m} = 0, \text{ if } \delta(k, m) > \Psi, \forall k, m \in \mathcal{V}. \quad (7)$$

Consequently, each element of the filtered signal, $\mathbf{H}\mathbf{x}$, is a linear combination of the signal elements in its Ψ -hop neighborhood. Hence, the filtered signal satisfies

$$[\mathbf{H}\mathbf{x}]_k = \sum_{m \in \mathcal{N}_\Psi[k]} H_{k,m} x_m, \quad (8)$$

where $\mathcal{N}_\Psi[k]$ is defined in (5). Thus, the filtered signal can be computed locally at each node by aggregating the values of the input signal within the Ψ -hop neighborhood of each of the nodes. We conclude with the following lemma.

Lemma 1. *Let, m and k be two nodes with a geodesic distance larger than 2Ψ , i.e. $\delta(k, m) > 2\Psi$. Then, their associated graph filter columns \mathbf{H}_m and \mathbf{H}_k are orthogonal, i.e.*

$$\mathbf{H}_m^T \mathbf{H}_k = 0. \quad (9)$$

Proof. First, we observe that

$$\mathbf{H}_m^T \mathbf{H}_k = \sum_{j \in \mathcal{V}} H_{m,j} H_{k,j}. \quad (10)$$

Additionally, the assumption that $\delta(k, m) > 2\Psi$ implies that there is no $j \in \mathcal{V}$ such that both $\delta(m, j) \leq \Psi$ and $\delta(k, j) \leq \Psi$. Hence, from (7), $\forall j \in \mathcal{V}$, at least one of the elements $H_{m,j}$ and $H_{k,j}$ is zero. Therefore, we obtain (9). \square

B. Assumptions on the Graphical Setting

In this paper, we consider the following assumptions on the underlying graph and the graph filter.

A.1 The maximum nodal degree (the maximal number of edges connected to one node) of the graph is considered small, i.e. $d_{\max} \ll |\mathcal{V}|$.

A.2 The graph filter is a polynomial of the GSO as defined in (6). Additionally, the graph filter degree, Ψ , is small with respect to (w.r.t.) the number of nodes, i.e. $\Psi \ll |\mathcal{V}|$.

The meaning of these assumptions is as follows. Assumption **A.1** enforces a sparse connectivity pattern on the underlying graph, i.e. *sparse graph*, where the number of edges is limited by $d_{\max}|\mathcal{V}|$, which is far fewer than the maximum possible number of edges $((1/2)|\mathcal{V}|(|\mathcal{V}| - 1))$. Furthermore, this sparse connectivity pattern is enforced uniformly in the sense that any subgraph of the graph is also sparse, where the restriction in Assumption **A.1** also applies to the subgraph. Assumption **A.2** restricts the number of elements in each Ψ -hop neighborhood by imposing a small value for Ψ . The structure of the polynomial graph filter shown in (6) also implies that, in general, the values of the filtered signal, $\mathbf{H}\mathbf{x}$, in (8), are more significant for indices associated with nodes closer to the nodes in Ω_t . Here, Ω_t refers to the support set of the sparse signal. Therefore, combining Assumptions **A.1-A.2** has a direct impact on the filtered signal outputs in (8), which are shown to be linear combinations of signal elements

in their Ψ -hop neighborhoods. Consequently, only a portion of the filtered signal outputs hold substantial information on the input signal.

The graph filter in (6) under Assumptions **A.1-A.2**, in addition to the sparsity restriction in (12), can be used to model a variety of GSP tasks, including signal reconstruction, blind deconvolution, sampling, and system identification [48]–[50], [60], [63]. Additionally, this framework can be used for modeling real-life applications in social networks [53], [54], biological networks [55], brain networks [67], epidemiology, computer networks [56], wireless sensor networks [5], and power systems [57], [58]. It is worth noting that in the context of power systems, the average nodal degree is generally very low (usually between 2 to 5) and does not increase with the network size [70]. This property is also common in other infrastructure systems, such as water and transportation systems.

C. Recovery of Sparse Graph Signals

In this paper, we aim to recover the source of a diffused sparse graph signal [48] from noisy observations under Assumptions **A.1-A.2**. That is, we are interested in recovering the graph signal \mathbf{x} , defined in (2), from the observation vector \mathbf{y} , where the following measurement model is assumed:

$$\mathbf{y} = \mathbf{H}\mathbf{x} + \mathbf{n}. \quad (11)$$

In this model, $\mathbf{H} \in \mathbb{R}^{|\mathcal{V}| \times |\mathcal{V}|}$ is the graph filter, defined in (6), which is a sparse dictionary matrix that satisfies Assumptions **A.1-A.2**. The noise is modeled by a $|\mathcal{V}| \times 1$ zero-mean Gaussian vector, \mathbf{n} , with a known covariance matrix, \mathbf{R} , i.e. $\mathbf{n} \sim \mathcal{N}(\mathbf{0}, \mathbf{R})$. Additionally, the unknown graph signal is assumed to be sparse:

$$\|\mathbf{x}\|_0 \leq s, \quad (12)$$

where $\|\cdot\|_0$ is the ℓ_0 semi-norm and the sparsity parameter s indicates the sparsity level. Hence, there exists a set of nodes, Ω_t , referred to as the signal support set such that

$$\mathbf{x}_k = 0, \forall k \in \{\mathcal{V} \setminus \Omega_t\}. \quad (13)$$

That is, only the elements in the support set Ω_t may correspond to non-zero elements of \mathbf{x} .

Based on (11)-(13), the sparse recovery problem can be formulated as (Eq. (1) in [20])

$$(\hat{\mathbf{x}}, \hat{\Omega}) = \arg \min_{|\Omega| \leq s} \min_{\mathbf{x}_\Omega \in \mathbb{R}^{|\Omega|}} \|\mathbf{y} - \mathbf{H}_\Omega \mathbf{x}_\Omega\|^2. \quad (14)$$

The inner minimization problem in (14) is a least squares (LS) problem with the solution (see, e.g. p. 225 in [71]):

$$\hat{\mathbf{x}}_\Omega = \arg \min_{\mathbf{x}_\Omega \in \mathbb{R}^{|\Omega|}} \|\mathbf{y} - \mathbf{H}_\Omega \mathbf{x}_\Omega\|^2 = (\mathbf{H}_\Omega^T \mathbf{H}_\Omega)^{-1} \mathbf{H}_\Omega^T \mathbf{y}. \quad (15)$$

By substituting (15) in (14) we obtain the following support set recovery problem:

$$\hat{\Omega} = \arg \min_{|\Omega| \leq s} \|\mathbf{y} - \mathbf{P}_{\mathbf{H}_\Omega} \mathbf{y}\|^2 = \arg \max_{|\Omega| \leq s} \|\mathbf{P}_{\mathbf{H}_\Omega} \mathbf{y}\|^2, \quad (16)$$

where $\mathbf{P}_{\mathbf{H}_\Omega}$ is the projection matrix onto the subspace $\text{col}(\mathbf{H}_\Omega)$, defined in (1). The last equality in (16) is obtained by using

the projection matrix property (see Theorem 2.22 in [72]):

$$\|\mathbf{y} - \mathbf{P}_{\mathbf{H}_\Omega} \mathbf{y}\|^2 = \|\mathbf{y}\|^2 - \|\mathbf{P}_{\mathbf{H}_\Omega} \mathbf{y}\|^2,$$

removing the constant $\|\mathbf{y}\|^2$, and rearranging the problem.

The support set recovery problem presented in (16) applies to any sparse signal \mathbf{x} and dictionary matrix \mathbf{H} , and is not restricted to graph-based settings. This formulation is valid as long as $\mathbf{H}_\Omega^T \mathbf{H}_\Omega$ is a nonsingular matrix. Therefore, we assume that for any support set Ω that satisfies $|\Omega| \leq s$, i.e. support that is relevant to our algorithms, the matrix \mathbf{H}_Ω has a full column rank. This problem can be viewed as a multiple-hypothesis testing problem, where under each hypothesis, the sparse signal has a different support set [73], which belongs to the following set of candidate sets:

$$\{\Omega \in \mathcal{V} : |\Omega| \leq s\}. \quad (17)$$

A direct solution of the support set recovery in (16) tends to overfit by selecting support sets with larger cardinality than the true support set. To mitigate this problem, we use the well-known GIC model selection method, which is a generalization of various criteria, such as the Akaike information criterion (AIC) and the minimum description length (MDL). For the considered problem, the GIC is given by [64]

$$\hat{\Omega} = \arg \max_{|\Omega| \leq s} \|\mathbf{P}_{\mathbf{H}_\Omega} \mathbf{y}\|^2 - \rho |\Omega|. \quad (18)$$

Compared to (16), the GIC in (18) includes an additional penalty function component, $\rho |\Omega|$, which depends on the support set cardinality. This penalty term mitigates the risk of overfitting; a larger penalty will lead to less complex models with a smaller support set, while a smaller penalty will result in a larger support set [64]. The penalty function can be tuned based on historical data, through trial and error, or by using model prior information. After solving (18), the sparse signal recovery solution can be obtained by substituting $\hat{\Omega}$ in (15).

In practice, an exact solution for (18) requires an exhaustive search over all $\sum_{j=1}^s \binom{|\mathcal{V}|}{j}$ optional support sets, which is infeasible. To overcome the unfeasibility of the combinatorial search, we propose using the graphical properties imposed by Assumptions A.1-A.2, and the *double sparsity* of the graph and the graph signal. The analysis for this setting is presented in Section III, and the proposed low-complexity support set recovery methods are developed in Section IV and Section V.

III. DICTIONARY MATRIX ANALYSIS

In this section, we analyze the dictionary matrix atoms (i.e. graph filter columns) based on the underlying graphical structure and Assumptions A.1-A.2. This analysis forms the basis for the proposed sparse recovery methods in Sections IV and V.

Taking into account that $x_k = 0$ for any $k \notin \Omega_t$, $k \in \mathcal{V}$ (see (13)), the filtered signal satisfies

$$\mathbf{H}\mathbf{x} = \mathbf{H}_{\Omega_t} \mathbf{x}_{\Omega_t} = \sum_{k \in \Omega_t} \mathbf{H}_k x_k, \quad (19)$$

where \mathbf{H}_k is the k th column of \mathbf{H} . Hence, the filtered signal, $\mathbf{H}\mathbf{x}$, can be viewed as a linear combination of dictionary atoms

(graph filter columns). Therefore, projecting the filtered signal into the single-column space $\text{col}(\mathbf{H}_m)$ results in

$$\mathbf{P}_{\mathbf{H}_m} \mathbf{H}\mathbf{x} = \sum_{k \in \Omega_t} \mathbf{P}_{\mathbf{H}_m} \mathbf{H}_k x_k, \quad (20)$$

where $\mathbf{P}_{\mathbf{H}_m}$ (defined in (1)) is a linear operator. Thus, it can be verified that

$$\mathbf{P}_{\mathbf{H}_m} \mathbf{H}\mathbf{x} = \mathbf{0} \text{ if } \mathbf{P}_{\mathbf{H}_m} \mathbf{H}_k = \mathbf{0}, \forall k \in \Omega_t. \quad (21)$$

In the following lemma, we show that $\mathbf{P}_{\mathbf{H}_m} \mathbf{H}_k = \mathbf{0}$ if the geodesic distance between k and m is larger than 2Ψ , $\delta(k, m) > 2\Psi$.

Lemma 2. *If two dictionary atoms correspond to nodes k and m with a geodesic distance larger than 2Ψ , i.e. $\delta(k, m) > 2\Psi$, then*

$$\mathbf{P}_{\mathbf{H}_m} \mathbf{H}_k = \mathbf{H}_m (\mathbf{H}_m^T \mathbf{H}_m)^{-1} \mathbf{H}_m^T \mathbf{H}_k = \mathbf{0}, \quad (22)$$

where $\mathbf{P}_{\mathbf{H}_m}$ is the projection matrix onto the single-column space $\text{col}(\mathbf{H}_m)$.

Proof: The first equality in (22) is obtained by substituting the definition of the projection matrix $\mathbf{P}_{\mathbf{H}_m}$. The second equality is obtained by substituting (9) from Lemma 1, since it is given that m and k satisfy $\delta(m, k) > 2\Psi$. ■

Leveraging the results in (19)-(22), we present the following definition and theorem.

Definition 1. *The Ψ -order neighborhood of the set Ω_t is*

$$\begin{aligned} \mathcal{N}_{2\Psi}[\Omega_t] &\triangleq \bigcup_{k \in \Omega_t} \mathcal{N}_{2\Psi}[k] \\ &= \{k \in \mathcal{V} : \exists m \in \Omega_t : 0 < \delta(k, m) \leq 2\Psi\}, \end{aligned} \quad (23)$$

where $\mathcal{N}_{2\Psi}[k]$ is defined in (5).

Theorem 3. *If $m \notin \mathcal{N}_{2\Psi}[k]$, then the following hold:*

$$\mathbf{P}_{\mathbf{H}_m} \mathbf{H}\mathbf{x} = \mathbf{0}, \quad (24a)$$

$$\mathbf{P}_{\mathbf{H}_m} \mathbf{y} = \mathbf{P}_{\mathbf{H}_m} \mathbf{H}\mathbf{x} + \mathbf{P}_{\mathbf{H}_m} \mathbf{n} = \mathbf{P}_{\mathbf{H}_m} \mathbf{n}, \quad (24b)$$

where $\mathbf{P}_{\mathbf{H}_m}$ is defined in (1) and \mathbf{y} is the measurement model defined in (11).

Proof: Since $m \notin \mathcal{N}_{2\Psi}[k]$, then Lemma 2 implies that $\mathbf{P}_{\mathbf{H}_m} \mathbf{H}_k = \mathbf{0}$, where each of the components in the summation satisfies $\mathbf{P}_{\mathbf{H}_m} \mathbf{H}_k x_k = \mathbf{0}$. Thus, we obtain (24a). Additionally, by left-multiplying the measurement model in (11) by $\mathbf{P}_{\mathbf{H}_m}$ and then substituting (24a) in the result, we obtain (24b). ■

It can be seen that Theorem 3 implies that the dictionary atoms indexed by nodes outside the set $\mathcal{N}_{2\Psi}[\Omega_t]$ in (23) contain only the contribution of the noise. That is, the dictionary matrix elements that contain information on the sparse graph signal are only those included in the 2Ψ neighborhood of Ω_t , $\mathcal{N}_{2\Psi}[\Omega_t]$. Thus, in practice, the true support of the signal is included in the set

$$\{\Omega \in \mathcal{N}_{2\Psi}[\Omega_t] : |\Omega| \leq s\}. \quad (25)$$

Consequently, we can significantly reduce the search set in (18) by using (25) instead of (17). This point is formalized in the following theorem, which establishes a bound on the

cardinality of the set $\mathcal{N}_{2\Psi}[\Omega_t]$ from (23) as a function of the graph filter degree Ψ , the graph structure, and the sparsity level s . This theorem provides constraints on the size of a reduced set of dictionary atoms that contain signal information. In particular, it offers two key advantages: first, it reduces the number of candidate support sets used to construct the feasible set in (18); second, in some cases, the node set, \mathcal{V} , could be divided into smaller subsets, enabling parallel processing.

Theorem 4. *The cardinality of the set $\mathcal{N}_{2\Psi}(\Omega)$ is bounded by*

$$|\mathcal{N}_{2\Psi}[\Omega_t]| \leq s \sum_{j=0}^{2\Psi} d_{\max}^j, \quad (26)$$

where d_{\max} is the maximum degree of the graph.

Proof. Since d_{\max} is the maximal degree of the graph, we obtain that each node in the graph has up to d_{\max} neighboring nodes, and each of those neighboring nodes can, in turn, have up to d_{\max} neighbors, and so on. As a result, the size of the 2Ψ neighborhood of a single node k satisfies

$$|\mathcal{N}_{2\Psi}[k]| \leq \sum_{j=0}^{2\Psi} d_{\max}^j. \quad (27)$$

By summing all the k th bounds in the form of (27) for $k \in \Omega_t$, we obtain

$$|\mathcal{N}_{2\Psi}[\Omega_t]| \leq \sum_{k=1}^{|\Omega_t|} |\mathcal{N}_{2\Psi}[k]| \leq \sum_{k=1}^{|\Omega_t|} \sum_{j=0}^{2\Psi} d_{\max}^j. \quad (28)$$

Therefore, since $|\Omega_t| \leq s$ under the sparsity assumption in (12), we conclude that the 2Ψ -neighborhood of Ω is bounded by the right hand side (r.h.s.) of (26). \square

The bound in (26) depends on the sparsity level, s , the maximal degree of the graph, d_{\max} , and the graph filter degree, Ψ , which are all considered to be small based on (12), Assumption A.1, and Assumption A.2, respectively. In contrast, the bound is independent of the size of the graph, i.e. the number of nodes, $|\mathcal{V}|$. Thus, for large networks it can be assumed that the bound is significantly lower than the actual number of nodes:

$$s \sum_{j=0}^{2\Psi} d_{\max}^j \ll |\mathcal{V}|. \quad (29)$$

Consequently, by substituting (29) in (26) we obtain

$$|\mathcal{N}_{2\Psi}[\Omega_t]| \ll |\mathcal{V}|. \quad (30)$$

The significance of the result in (30) lies in the observation that the number of dictionary atoms containing information about the sparse signal is much smaller than the total number of dictionary atoms that are required for searching for the optimal GIC in (18). As a result, any sparse recovery method that employs a search algorithm (and not just the GIC in (18)) can significantly reduce its computational complexity by focusing on the reduced set of dictionary atoms associated with the nodes in $\mathcal{N}_{2\Psi}[\Omega_t]$ instead of on the entire set associated with all nodes in \mathcal{V} .

Moreover, it should be noted that the bound in (26) is not tight. This is because we may have overlaps between the Ψ -order neighborhoods of the nodes in Ω_t and overlaps within the Ψ -order neighborhoods of individual nodes (see first and second inequalities in (28), respectively). As a result, in practice, the number of elements in $\mathcal{N}_{2\Psi}[\Omega_t]$ can be considerably lower than its bound in (26). This further emphasizes the advantage of reducing computational complexity by searching over $\mathcal{N}_{2\Psi}[\Omega_t]$ instead of \mathcal{V} .

Dictionary atoms within the set $\mathcal{N}_{2\Psi}(\Omega_t)$ may differ in the significance of the information they provide about the signal. Specifically, some dictionary atoms might convey less relevant information compared to others, with some containing only minor details that are less significant in the context of the signal. To remove the less informative dictionary atoms, we define the subset \mathcal{D} as including only those dictionary atoms that offer substantial information about the signal.

Definition 2. *Let $\epsilon > 0$ be a tuning parameter. Then, the set $\mathcal{D} \subset \mathcal{N}_{2\Psi}(\Omega_t)$ is defined such that*

$$\|\mathbf{P}_{\mathbf{H}_m} \mathbf{H}_{\Omega_t} \mathbf{x}_{\Omega_t}\|_2^2 < \epsilon, \quad \forall m \in \{\mathcal{N}_{2\Psi}(\Omega_t) \setminus \mathcal{D}\}. \quad (31)$$

The definition of the set \mathcal{D} is determined by the parameter ϵ , introducing a fundamental trade-off. A larger value of ϵ will result in a smaller set \mathcal{D} , which may improve the computational efficiency of the proposed sparse recovery algorithms. However, this can also lead to the exclusion of dictionary atoms containing significant signal information from the set \mathcal{D} , thereby degrading the overall recovery performance. Conversely, selecting a smaller value of ϵ results in a larger set \mathcal{D} , potentially reaching the extreme case where $\mathcal{D} = \mathcal{N}_{2\Psi}(\Omega_t)$. In this scenario, the size of the search space and the computational overhead are not effectively reduced. In addition, the choice of ϵ can ensure the existence of a non-empty set \mathcal{D} . Thus, careful tuning of ϵ is crucial. One approach is to set ϵ based on the signal-to-noise ratio (SNR), ensuring that atoms with contributions comparable to the noise variance are excluded from \mathcal{D} . Another strategy is to leverage prior information, if available, to guide the selection of ϵ .

Using the set \mathcal{D} instead of the entire node set \mathcal{V} for the objective function in (18), i.e. searching over $\{\Omega \subset \mathcal{D} : |\Omega| \leq s\}$, offers significant advantages in some scenarios, depending on the sparsity pattern of the signal. In these scenarios, reducing the search space may enable the partitioning of \mathcal{D} into subsets, $\{\mathcal{D}_q\}_q$ that are associated with dictionary atoms spanning orthogonal subspaces, as detailed in Section IV-A1. In this case, the search set can be divided w.r.t. the partition to smaller search sets: $\{\{\Omega \subset \mathcal{D}_q : |\Omega| \leq s\}\}_q$. This strategic partitioning facilitates parallel processing, which enhances the computational efficiency during the search over \mathcal{D} .

IV. SPARSE RECOVERY OF GRAPH SIGNALS

In this section, we propose two methods for solving the GIC support set recovery problem in (18) under the GSP measurement model in (11). The analysis in Section III provides the basis for these methods, since it enables searching for the optimal support set over a reduced set of dictionary atoms. In Subsection IV-A, we present the GM-GIC method, which

involves a node partitioning followed by the implementation of the GIC locally on each partitioned subset. In Subsection IV-B, we present the Graph-BNB-GIC method, which is based on the BNB method [65], [66], and involves an upper bound that is derived based on the underlying graphical structure, thus significantly enhancing the traceability of this method.

A. GM-GIC

In this subsection, we outline the rationale and then present the methodology of the GM-GIC method.

1) Node partition

The analysis in Section III implies that the true support set of the signal, Ω_t , is included in the set \mathcal{D} from (31). We define the following partition on the set \mathcal{D} , $\{\mathcal{D}_q\}_{q=1}^Q$, such that

$$d_{\mathcal{G}}(k, m) > 2\Psi, \quad \forall k \in \mathcal{D}_q, \quad \forall m \in \mathcal{D}_{q'}, \quad (32)$$

for any two subsets \mathcal{D}_q and $\mathcal{D}_{q'}$ from $\{\mathcal{D}_q\}_{q=1}^Q$, where $q \neq q'$ and $1 \leq Q \leq s$. The partial support set in the q th area, denoted as Ω_q , is defined as $\Omega_q = \{\Omega_t \cap \mathcal{D}_q\}$. It should be noted that $\{\Omega_q\}_{q=1}^Q$ is a *partition* of the true support set Ω_t , since there is no overlap between these subsets and $\Omega_t = \bigcup_{q=1}^Q \Omega_q$.

Based on (9) in Lemma 1, the partition in (32) implies that any two dictionary atoms associated with two elements from two different subsets are orthogonal, i.e.

$$\mathbf{H}_m^T \mathbf{H}_k = 0, \quad \forall k \in \mathcal{D}_q, \quad \forall m \in \mathcal{D}_{q'}, \quad (33)$$

for any q' and q where $q \neq q'$. Hence, by definition, the column spaces associated with two different subsets are orthogonal, i.e. $\text{col}(\mathbf{H}_{\mathcal{D}_q}) \perp \text{col}(\mathbf{H}_{\mathcal{D}_{q'}})$. Therefore, the projection of $\mathbf{H}_{\Omega_q} \mathbf{x}_{\Omega_q}$, where $\Omega_q = \{\Omega_t \cap \mathcal{D}_q\}$, onto $\text{col}(\mathbf{H}_{\mathcal{D}_{q'}})$ satisfies

$$\mathbf{P}_{\mathbf{H}_{\mathcal{D}_{q'}}} \mathbf{H}_{\Omega_q} \mathbf{x}_{\Omega_q} = \mathbf{0}, \quad (34)$$

for any q' and q where $q \neq q'$. This implies that the partial support set $\Omega_q \subset \mathcal{D}_q$ does not affect the measurements in other subsets $\mathcal{D}_{q'}$, $q' = 1, \dots, Q, q' \neq q$. Thus, instead of searching for the true support set, Ω_t , over the entire set \mathcal{D} , we aim to find the partial support sets, $\{\Omega_q\}_{q=1}^Q$, by searching across the smaller subsets $\{\mathcal{D}_q\}_{q=1}^Q$. In Algorithm 1 presents an algorithm to partition \mathcal{D} to connected sets that satisfy (32).

Algorithm 1: Node Partitioning

Input: Graph $\mathcal{G}(\mathcal{V}, \mathcal{E})$, node subset \mathcal{D}

- 1 Set $\tilde{\mathcal{V}} = \mathcal{D}$ % new node set
- 2 Set % new edge set

$$\tilde{\mathcal{E}} = \{(k, m) : k, m \in \tilde{\mathcal{V}}, 1 \leq \delta(k, m) \leq 2\Psi\} \quad (35)$$

Generate a partition of $\tilde{\mathcal{G}}(\tilde{\mathcal{V}}, \tilde{\mathcal{E}})$ with connected components (e.g. using *conncomp* in Matlab)

- 3 **Return** subsets $\{\mathcal{D}_q\}_{q=1}^Q$, where \mathcal{D}_q includes the nodes in the q th connected component obtained from the graph partition.
-

Claim 1. The subsets $\{\mathcal{D}_q\}_{q=1}^Q$ obtained from Algorithm 1 satisfy (32).

Proof: Let $\{\mathcal{D}_q\}_{q=1}^Q$ be the subsets obtained from Algorithm 1, and let k and m be selected from different subsets. For the sake of contradiction, assume that $\delta(k, m) \leq 2\Psi$. Since k and m satisfy $\delta(k, m) \leq 2\Psi$, they must be connected by one of the edges in the set $\tilde{\mathcal{E}}$, i.e. $(k, m) \in \tilde{\mathcal{E}}$, where $\tilde{\mathcal{E}}$ is defined in (35). However, this contradicts our assumption since $(k, m) \in \tilde{\mathcal{E}}$ only if k and m are in the same connected component \mathcal{D}_q . Therefore, we can conclude that when k and m are in different subsets from $\{\mathcal{D}_q\}_{q=1}^Q$, then the geodesic distance between them satisfies $\delta(k, m) > 2\Psi$. Correspondingly, the subsets obtained from Algorithm 1 satisfy (32). ■

The node partitioning presented in this subsection is used in the GM-GIC method in Subsection IV-A2 in order to reduce the amount of required computations without compromising the estimation performance. When partitioning is not possible (i.e. when $Q = 1$), GM-GIC method still offers an advantage over the GIC method by performing an exhaustive search over \mathcal{D} , which is a smaller subset of the overall node set \mathcal{V} . Moreover, when $Q > 1$, partitioning the subset \mathcal{Q} into smaller subsets $\{\mathcal{D}_q\}_q$ enables the exhaustive search to be conducted on these smaller subsets, as illustrated in Fig. 1.

2) Methodology

The GM-GIC method consists of four steps. In the **first step**, based on (24b), we estimate the set \mathcal{D} described in (31) by applying the generalized likelihood ratio test (GLRT) for each $m \in \mathcal{V}$ on the following binary hypothesis testing problem:

$$\begin{cases} \mathcal{H}_0 : \mathbf{P}_{\mathbf{H}_m} \mathbf{y} = \mathbf{P}_{\mathbf{H}_m} \mathbf{n} \\ \mathcal{H}_1 : \mathbf{P}_{\mathbf{H}_m} \mathbf{y} = \mathbf{P}_{\mathbf{H}_m} \mathbf{H} \mathbf{x} + \mathbf{P}_{\mathbf{H}_m} \mathbf{n}. \end{cases} \quad (36)$$

This hypothesis testing can be understood as the task of detecting a signal embedded in Gaussian noise. In this case, the signal is projected onto a smaller subspace, $\mathbf{P}_{\mathbf{H}_m} \mathbf{y}$, under both hypotheses. Under \mathcal{H}_1 , the signal is presumed to be present in the subspace, whereas in \mathcal{H}_0 the subspace encompasses solely the noise.

The GLRT for the hypothesis testing in (36) is defined for each $m \in \mathcal{V}$ as (see, e.g. p. 201 in [74])

$$\|\mathbf{P}_{\mathbf{H}_m} \mathbf{y}\|^2 \underset{\mathcal{H}_0}{\overset{\mathcal{H}_1}{\gtrless}} \zeta, \quad (37)$$

where ζ is a user-defined threshold parameter. This threshold is closely related to the parameter ϵ from the definition of the set \mathcal{D} in (31). However, while ϵ is associated with the filtered signal $\mathbf{H} \mathbf{x}$ (see in (31)), ζ is applied to the measurement vector \mathbf{y} (see in (37)) and, thus, also accounts for the measurement noise. Thus, the set \mathcal{D} is estimated according to the binary detector in (37), which is defined for each $m \in \mathcal{V}$, by

$$\hat{\mathcal{D}} \triangleq \{m \in \mathcal{V} : \|\mathbf{P}_{\mathbf{H}_m} \mathbf{y}\|^2 > \zeta\}. \quad (38)$$

In the **second step**, we use the node partition algorithm in Algorithm 1 with the input $\hat{\mathcal{D}}$ from (38) to obtain the subsets $\{\hat{\mathcal{D}}_q\}_{q=1}^Q$. In the **third step**, we solve the support set recovery problem in (18) for each subset $\hat{\mathcal{D}}_q$ separately. That is, we estimate the partial support set by

$$\hat{\Omega}_q = \arg \max_{\{|\Omega| \leq s, \Omega \subseteq \hat{\mathcal{D}}_q\}} \|\mathbf{P}_{\mathbf{H}_{\Omega}} \mathbf{y}\|^2 - \rho |\Omega|, \quad q = 1, \dots, Q. \quad (39)$$

It is noted that for any $q = 1, \dots, Q$, the partial support set, $\hat{\Omega}_q$, may be smaller than or equal to the subset from which it is recovered, $\hat{\mathcal{D}}_q$. The total support set of the sparse vector is then computed as the union of the partial estimates obtained from (39), as follows:

$$\hat{\Omega}^{temp} = \bigcup_{q=1}^Q \hat{\Omega}_q. \quad (40)$$

It should be noted that in (39) we impose the condition that the size of the support set should not exceed the sparsity parameter, $|\Omega| \leq s$, for each subset separately. As a result, we can ensure that the cardinality of $\hat{\Omega}_q$ is always less than or equal to s for any $q = 1, \dots, Q$. However, the same restriction does not apply to the union set in (40), which means that the cardinality of $\hat{\Omega}^{temp}$ may be greater than s , and thus, it may not be in the feasible set of the original optimization problem in (18). In order to address this issue, in the **fourth step**, sparsity-level correction is performed by solving the recovery in (16) for $\{\Omega \subset \hat{\Omega}^{temp} : |\Omega| \leq s\}$. That is, we compute the final estimator of the support set by

$$\hat{\Omega} = \arg \max_{\{\Omega \subset \hat{\Omega}^{temp} : |\Omega| \leq s\}} \|\mathbf{P}_{\mathbf{H}_\Omega} \mathbf{y}\|^2 - \rho|\Omega|. \quad (41)$$

The GM-GIC method is summarized in Algorithm 2 and illustrated in Fig. 1.

Algorithm 2: GM-GIC

Input: Measurements \mathbf{y} , graph filter \mathbf{H} , filter degree Ψ , and sparsity parameter s

- 1 Step 1: Compute $\hat{\mathcal{D}}$ from (38)
 - 2 Step 2: Partition $\hat{\mathcal{D}}$ by Algorithm 1 to obtain $\{\hat{\mathcal{D}}_q\}_{q=1}^Q$
 - 3 Step 3:
 - 3 **for** $q = 1$ **to** Q **do**
 - 4 Obtain $\hat{\Omega}_q$ by solving (39)
 - 5 **end**
 - 6 Compute: $\hat{\Omega}^{temp} = \bigcup_{q=1}^Q \hat{\Omega}_q$
 - 7 Step 4:
 - 7 Obtain $\hat{\Omega}$ by solving (41).
 - 8 **Return** *recovered support*: $\hat{\Omega}$
-

B. Graph-BNB-GIC

In this subsection we present a new Graph-BNB-GIC method for solving the GIC problem in (18). To this end, we reformulate the GIC problem in (18) as an integer programming optimization problem, and then derive the Graph-BNB-GIC method. The Graph-BNB-GIC, is a BNB-based method (see, e.g. [65], [66]) with novel graph-based designs for the branching and bounding steps.

1) New formulation

By using the $|\mathcal{V}| \times 1$ Boolean vector $\mathbf{z} = [z_1, \dots, z_{|\mathcal{V}|}]^T$, we address the GIC problem in (18) as the following integer programming optimization problem:

$$\begin{aligned} \hat{\mathbf{z}} = \arg \max_{\mathbf{z} \in \{0,1\}^{|\mathcal{V}|}} & \|\mathbf{P}_{\mathbf{H}_{\Omega(\mathbf{z})}} \mathbf{y}\|^2 - \rho|\Omega(\mathbf{z})| \\ \text{such that } & |\Omega(\mathbf{z})| \leq s, \end{aligned} \quad (42)$$

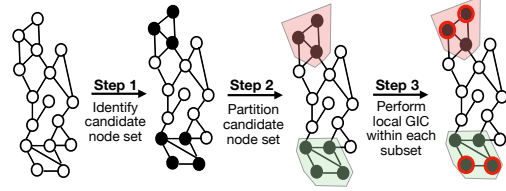


Figure 1: Steps 1-3 of the GM-GIC method from Algorithm 2. In Step 1, the algorithm estimates the candidate node set, \mathcal{D} , denoted by black-filled nodes. A node k is included in \mathcal{D} if the projection of the measurements into the single-column space $\text{col}(\mathbf{H}_k)$, $\|\mathbf{P}_{\mathbf{H}_k} \mathbf{y}\|^2$, exceeds a certain threshold. In Step 2, the nodes in \mathcal{D} are partitioned into subsets (here, 2 subsets in pink and green) based on the geodesic distance between the nodes, the graph filter order, and the graph structure. Finally, in Step 3, a local GIC is performed for the support set recovery within the subsets. This results in separate partial support sets (denoted by red rings around the nodes).

where $\Omega(\mathbf{z})$ is the support set of \mathbf{z} , i.e. the set of indices corresponding to non-zero elements of \mathbf{z} that are in this case equal to 1. It can be verified that the problem in (42) is equivalent to the problem in (18) (provides the same solution). In the new formulation, each node k can be fixed to either $z_k = 0$ or $z_k = 1$. In this way we can impose additional information on the specific node, and determine whether it is part of the support set or not. The added flexibility is essential for the *branch step*, which is described next.

2) Branch

Without loss of generality, we assume that the graph node indices are ordered according to their single-node projected energy, i.e.

$$\|\mathbf{P}_{\mathbf{H}_1} \mathbf{y}\|_2^2 \geq \|\mathbf{P}_{\mathbf{H}_2} \mathbf{y}\|_2^2 \geq \dots \geq \|\mathbf{P}_{\mathbf{H}_{|\mathcal{V}|}} \mathbf{y}\|_2^2. \quad (43)$$

According to the discussion around (31), nodes included in the true support set of the signal \mathbf{x} , Ω_t , are associated with smaller indices in (43). Moreover, dictionary atoms associated with nodes indexed larger than $|\mathcal{D}|$, w.r.t. to the ordering in (43), are not expected to contain substantial information on the filtered signal, $\mathbf{H}\mathbf{x}$. Based on the ordering in (43), we describe the *branch step* as follows. By selecting index 1, we form the following two problems: the first problem is

$$\begin{aligned} \hat{\mathbf{z}} = \arg \max_{\mathbf{z} \in \{0,1\}^{|\mathcal{V}|}} & \|\mathbf{P}_{\mathbf{H}_{\Omega(\mathbf{z})}} \mathbf{y}\|^2 - \rho|\Omega(\mathbf{z})| \\ \text{such that } & \begin{cases} |\Omega(\mathbf{z})| \leq s \\ z_1 = 0, \end{cases} \end{aligned} \quad (44)$$

and the second problem is

$$\begin{aligned} \hat{\mathbf{z}} = \arg \max_{\mathbf{z} \in \{0,1\}^{|\mathcal{V}|}} & \|\mathbf{P}_{\mathbf{H}_{\Omega(\mathbf{z})}} \mathbf{y}\|^2 - \rho|\Omega(\mathbf{z})| \\ \text{such that } & \begin{cases} |\Omega(\mathbf{z})| \leq s \\ z_1 = 1. \end{cases} \end{aligned} \quad (45)$$

In other words, we fix the value of z_1 to 0 in the first subproblem, which means that the first node is not part of $\Omega(\mathbf{z})$. In the second subproblem, we set the value of z_1 to be 1, which means that the first node is part of $\Omega(\mathbf{z})$. The problems

in (44) and (45) are subproblems of the original problem in (42) since they have the same cost function and constraints as the original problem with one additional variable fixed. Each of these subproblems is an integer programming optimization problem, with $|\mathcal{V}| - 1$ Boolean variables. The optimal value of the original problem is the maximum between the optimal values of the two subproblems.

The division of (42) to the two subproblems in (44)-(45) is the first *branch step* performed in our algorithm. The second *branch step* is obtained by splitting one of the above subproblems, once with $z_2 = 0$ and once with $z_2 = 1$, following the order in (43). By continuing in this manner, we form a partial binary tree of subproblems (see our illustration in Fig. 2). The root is the original problem depicted in (42). This problem is split into the two child subproblems in (44) and (45). The second iteration yields another two children of one of the original children. In general, the subproblems can be written as

$$\hat{\mathbf{z}} = \arg \max_{\mathbf{z} \in \{0,1\}^{|\mathcal{V}|}} \|\mathbf{P}_{\mathbf{H}_{\Omega(\mathbf{z})}} \mathbf{y}\|^2 - \rho |\Omega(\mathbf{z})|$$

such that $\begin{cases} |\Omega(\mathbf{z})| \leq s \\ z_k = 0, \quad k \in \mathcal{S}_0 \\ z_k = 1, \quad k \in \mathcal{S}_1, \end{cases} \quad (47)$

where \mathcal{S}_0 is the set of Boolean variables fixed to 1 and \mathcal{S}_1 is the set of Boolean variables fixed to 0. It can be seen that in the optimization problem in (47), the equality constraints determine $|\mathcal{S}_0| + |\mathcal{S}_1|$ from the elements of \mathbf{z} . Hence, each subproblem could be represented by the notation $(\mathcal{S}_0, \mathcal{S}_1)$, e.g. (\emptyset, \emptyset) , $(\{1\}, \emptyset)$, and $(\emptyset, \{1\})$ represent (42), (44), and (45), respectively. Additionally, splitting (47) into two subproblems is achieved by adding node $|\mathcal{S}_0| + |\mathcal{S}_1| + 1$ once to the set \mathcal{S}_0 and once to the set \mathcal{S}_1 . Hence, the index used to split a leaf node is determined based on the ordering in (43), where a leaf node refers to a node in the partial binary tree that does not have children nodes. Figure 2 illustrates two iterations of the *branch step*.

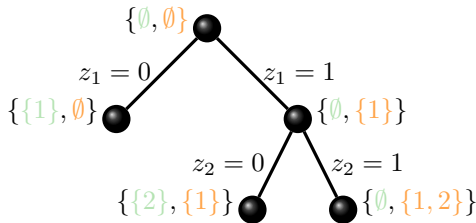


Figure 2: Illustration of two iterations of the *branch step*. Each node (black circle) corresponds to an optimization problem in (47), and is identified by the couple $\{\mathcal{S}_0, \mathcal{S}_1\}$, that are assumed to be **included in/excluded from** the support set, respectively.

3) Bound

When applied to large models, standard BNB search algorithms (see e.g. [65]) that use theoretical upper and lower bounds may take substantial amounts of computing time for mixed Boolean convex problems. Using a heuristic bound to replace the upper or lower bound might achieve a significant speedup in the BNB search procedure. For example, [75], [76]

showed, for the optimal network design problem, that using a heuristic bound may dramatically reduce the computational complexity with a minor effect on the performance. Therefore, based on the analysis in Subsection III, we propose a heuristic upper bound alongside a theoretical lower bound for (47).

Based on the analysis in Subsection III, which stems from Assumptions A.1-A.2, we propose the following heuristic upper bound on the optimal objective of (47):

$$\Phi_{ub}(\mathcal{S}_0, \mathcal{S}_1) = \|\mathbf{P}_{\mathbf{H}_{\mathcal{S}_1}} \mathbf{y}\|^2 - \rho |\mathcal{S}_1| + (s - |\mathcal{S}_1|) \max \left(\|\mathbf{P}_{\mathbf{H}_{k+1}} \mathbf{y}\|^2 - \rho(1), 0 \right), \quad (48)$$

where $k = |\mathcal{S}_0| + |\mathcal{S}_1|$. The heuristic bound states that the maximum cost function in (47) is bounded by the superposition of:

- 1) The cost function associated with the elements in \mathbf{z} that are already fixed as 1 (the elements in \mathcal{S}_1): $\|\mathbf{P}_{\mathbf{H}_{\mathcal{S}_1}} \mathbf{y}\|^2 - \rho |\mathcal{S}_1|$;
- 2) The cost function associated with the highest individual contributor within the elements not yet determined, i.e. node $k + 1$ where $k = |\mathcal{S}_0| + |\mathcal{S}_1|$, multiplied by the number of elements that can be added to \mathcal{S}_1 without exceeding the sparsity limit: $(s - |\mathcal{S}_1|) \max \left(\|\mathbf{P}_{\mathbf{H}_{k+1}} \mathbf{y}\|^2 - \rho(1), 0 \right)$.

The lower bound on the optimal solution of (47) is obtained by taking the cost function of one of the elements in the feasible set. Specifically, we consider the element \mathbf{z} in which the undetermined elements (i.e., the elements in $\{\mathcal{V} \setminus \{\mathcal{S}_0\} \cup \mathcal{S}_1\}$) are set to zero. All the elements in \mathbf{z} are determined for this case, and the non-zero elements correspond to the set \mathcal{S}_1 . Thus, the lower bound for (47) is set to

$$\Phi_{lb}(\mathcal{S}_1) = \|\mathbf{P}_{\mathbf{H}_{\mathcal{S}_1}} \mathbf{y}\|^2 - \rho |\mathcal{S}_1|. \quad (49)$$

Hence, the lower bound for (47) is equivalent to the cost function of the support set $\Omega = \mathcal{S}_1$. It is noted that the lower bound used is a valid bound that is always lower than the optimal value of the solution of (47). This can be verified by observing the fact that $\Omega(\mathbf{z}) = \mathcal{S}_1$ is in the feasible set of the maximization problem in (47), and thus its cost would always be lower than or equal to the optimal cost function.

4) Remarks

We conclude the discussion on the bounds with the following two remarks that demonstrate the relationships between the lower and upper bounds in special cases.

Remark 1. By substituting (49) in (48) we obtain

$$\Phi_{ub}(\mathcal{S}_0, \mathcal{S}_1) = \Phi_{lb}(\mathcal{S}_1) + (s - |\mathcal{S}_1|) \max \left(\|\mathbf{P}_{\mathbf{H}_{k+1}} \mathbf{y}\|^2 - \rho, 0 \right). \quad (50)$$

Thus, if $|\mathcal{S}_1| = s$, then the lower bound and upper bound are equal, i.e., $\Phi_{ub}(\mathcal{S}_0, \mathcal{S}_1) = \Phi_{lb}(\mathcal{S}_1)$. The rationale behind this result is that in this case, the subproblem already reaches the maximal support set cardinality, s , and, thus, the associated leaf node in the binary tree should not be further divided.

Remark 2. Due to the ordering in (43), it can be verified that if $k > |\mathcal{D}|$, then $k \in \{\mathcal{V} \setminus \mathcal{D}\}$. Hence, from (31) we obtain that

$\|\mathbf{P}_{\mathbf{H}_k} \mathbf{H}_{\Omega_t} \mathbf{x}_{\Omega_t}\| < \epsilon$. Thus, if the noise variance is negligible compared to the filtered signal, it can be assumed that

$$\|\mathbf{P}_{\mathbf{H}_{k+1}} \mathbf{y}\|^2 - \rho < \epsilon, \quad (51)$$

where ρ is the GIC penalty parameter in (18). By substituting the result from (51) in (50), we obtain that the difference between the upper and lower bound in (50) when $k > |\mathcal{D}|$ satisfies

$$\Phi_{ub}(\mathcal{S}_0, \mathcal{S}_1) - \Phi_{lb}(\mathcal{S}_1) < (s - |\mathcal{S}_1|)\epsilon < s\epsilon,$$

where the sparsity parameter s indicates the sparsity level of the signal, \mathbf{x} , and ϵ is defined in (31). This result implies that observing support set elements with nodes outside \mathcal{D} cannot improve the support set recovery results. Consequently, the result shows that in the worst-case scenario of the algorithm, it terminates after observing all support set combinations within the set \mathcal{D} from (31). Hence, in its worst case, the algorithm requires an order of $O\left(\sum_{j=1}^s \binom{|\mathcal{D}|}{j}\right)$ flops (see Subsection IV-C for a comparison with the GIC and GM-GIC methods).

5) Algorithm

The algorithm for implementing the Graph-BNB-GIC method is initialized by the set $\mathcal{L}^{(0)}$ containing only the root node, which is characterized by the sets $(\mathcal{S}_0, \mathcal{S}_1) = (\emptyset, \emptyset)$. At each iteration, branching occurs from the leaf node with the smallest depth, where if there are multiple leaves with the smallest depth, then the leaf with the largest upper bound is selected. That is, the leaf node is selected by

$$(\hat{\mathcal{S}}_0, \hat{\mathcal{S}}_1) = \arg \max_{(\mathcal{S}_0, \mathcal{S}_1) \in \mathcal{L}^{(t)}} \Phi_{ub}(\mathcal{S}_0, \mathcal{S}_1),$$

such that $|\mathcal{S}_0| + |\mathcal{S}_1| = \min_{(\tilde{\mathcal{S}}_0, \tilde{\mathcal{S}}_1) \in \mathcal{L}^{(t)}} |\tilde{\mathcal{S}}_0| + |\tilde{\mathcal{S}}_1|. \quad (52)$

The branching is performed by the *branch step* outlined in Subsection IV-B2. Hence, to generate $\mathcal{L}^{(t+1)}$, all elements in $\mathcal{L}^{(t)}$ are duplicated excluding the selected leaf node. The sets of the selected node, $(\mathcal{S}_0, \mathcal{S}_1)$, are then split into two child nodes: $(\{\mathcal{S}_0 \cup k\}, \mathcal{S}_1)$ and $(\mathcal{S}_0, \{\mathcal{S}_1 \cup k\})$, where $k = |\mathcal{S}_0| + |\mathcal{S}_1|$. The algorithm terminates when $L^{(t+1)} = U^{(t+1)}$, where $U^{(t+1)}$ and $L^{(t+1)}$ denote the maximum upper bound and maximum lower bound across all leaf nodes (nodes in $\mathcal{L}^{(t+1)}$), respectively. In this case, the maximum upper bound and maximum lower bound belong to the same leaf, and the set \mathcal{S}_1 , which is associated with this leaf, represents the estimated support set (i.e. the algorithm output). Additionally, if the upper bound of a leaf is smaller than the global lower bound, $L^{(t+1)}$, then it is pruned (removed from the set $\mathcal{L}^{(t+1)}$) since the cost function associated with any of its potential descendants is assumed lower than its upper bound and that the global lower bound represents a cost function of a feasible solution. The proposed Graph-BNB-GIC method is summarized in Algorithm 3.

C. Computational Complexity

The main goal of this work is to develop graph-based low-complexity methods for support set recovery of sparse graph signals. Specifically, we aim to design low-complexity methods that approximate the solution of the GIC optimization

Algorithm 3: Graph-BNB-GIC

Input: Measurements \mathbf{y} , graph filter \mathbf{H} , and sparsity parameter s

```

1 Index  $\mathcal{V}$  by (43)
2 Initialize:
3  $t = 0$ ,  $\mathcal{L}^{(0)} = \{(\emptyset, \emptyset)\}$ 
4 Compute:  $L^{(0)} = \Phi_{lb}(\emptyset)$ ,  $U^{(0)} = \Phi_{ub}(\emptyset, \emptyset)$ 
5 while  $L^{(t)} < U^{(t)}$  do
6   Pick  $(\mathcal{S}_0, \mathcal{S}_1)$  by (52)
7   Set  $k = |\mathcal{S}_0| + |\mathcal{S}_1|$ ,  $\mathcal{L}^{(t+1)} = \mathcal{L}^{(t)}$ 
8   % Branching  $(\mathcal{S}_0, \mathcal{S}_1)$ : (lines 8-10)
9   Set  $\mathcal{L}^{(t+1)} = \{\mathcal{L}^{(t+1)} \setminus (\mathcal{S}_0, \mathcal{S}_1)\}$ 
10  Set  $\mathcal{L}^{(t+1)} = \{\mathcal{L}^{(t+1)} \cup (\{\mathcal{S}_0 \cup k\}, \mathcal{S}_1)\}$ 
11  Set  $\mathcal{L}^{(t+1)} = \{\mathcal{L}^{(t+1)} \cup (\mathcal{S}_0, \{\mathcal{S}_1 \cup k\})\}$ 
12  Compute:  $L^{(t+1)} = \arg \max_{(\mathcal{S}_0, \mathcal{S}_1) \in \mathcal{L}^{(t+1)}} \Phi_{lb}(\mathcal{S}_1)$ 
13  Compute:  $U^{(t+1)} = \arg \max_{(\mathcal{S}_0, \mathcal{S}_1) \in \mathcal{L}^{(t+1)}} \Phi_{ub}(\mathcal{S}_0, \mathcal{S}_1)$ 
14  Pruning: remove  $(\mathcal{S}_0, \mathcal{S}_1) \in \mathcal{L}^{(t+1)}$  if it satisfies
       $\Phi_{ub}(\mathcal{S}_0, \mathcal{S}_1) < L^{(t+1)}$ 
15  Update:  $t = t + 1$ 
16 end
17 Return recovered support set  $\hat{\Omega} = |\mathcal{S}_1|$  such that
       $(\mathcal{S}_0, \mathcal{S}_1) \in \mathcal{L}^{(t)}$  and  $\Phi_{lb}(\mathcal{S}_1) = L^{(t)}$ 

```

in (18), since a direct solution requires an exhaustive search with computational complexity that grows exponentially with the size of the graph. In particular, the exhaustive search requires $\sum_{j=1}^s \binom{|\mathcal{V}|}{j}$ floating-point operations (flops), as can be seen in (18). The computational complexity of the GM-GIC method from Algorithm 2 is primarily determined by the computations of the local GIC on the largest subset, and thus requires $O\left(\sum_{j=1}^s \binom{\max_q |\mathcal{D}_q|}{j}\right)$ flops. In particular, when the set \mathcal{D} cannot be partitioned, the complexity becomes $O\left(\sum_{j=1}^s \binom{|\mathcal{D}|}{j}\right)$. Hence, its complexity is significantly lower than those of the GIC methods, where $\forall q : \mathcal{D}_q \subseteq \mathcal{D}$ and from (31) and Theorem 4, $|\mathcal{D}| \ll |\mathcal{V}|$. The Graph-BNB-GIC method from Algorithm 3 is anticipated to have an even lower computational burden compared with the GM-GIC method, due to its iterative nature. However, as shown in Remark 2, in its worst-case scenario it requires an order of $O\left(\sum_{j=1}^s \binom{|\mathcal{D}|}{j}\right)$ flops. Consequently, even in the worst case, the computational complexity of the Graph-BNB-GIC method is significantly lower than that of the GIC method. This analysis highlights that the main advantage of the proposed methods lies in their reliance on the size of the set \mathcal{D} for complexity considerations, rather than the size of the entire node set, \mathcal{D} , thereby enabling efficient computation even in large-scale applications.

V. GFOC

In this section, we present the GFOC method, which is a new method for correcting existing estimated support sets of the sparse graph signal, $\hat{\Omega}$. This correction is obtained by optionally replacing the support set elements with nodes

from their one-hop neighborhood, $\mathcal{N}[\hat{\Omega}]$. The initial estimated support set, $\hat{\Omega}$, can be obtained by any sparse recovery method, including standard techniques (such as the OMP [31] and Lasso [23] methods), as well as the GM-GIC and Graph-BNB-GIC methods proposed in Section IV.

A. Method

The proposed GFOC method receives as an input a support set estimate, $\hat{\Omega}$, provided by any sparse recovery algorithm, along with the system measurements and the information regarding the underlying graph. Then, the GFOC method goes over the estimated support set elements. For each element (i.e. each node $k \in \hat{\Omega}$), it examines whether the GIC increases when the element is replaced with one of the nodes in the one-hop open neighborhood set

$$\mathcal{N}(k) \triangleq \{\mathcal{N}_1[k] \setminus k\} = \{m \in \mathcal{V} : \delta(k, m) = 1\}, \quad (53)$$

where $\mathcal{N}_1[k]$ is defined in (5) (with $\Delta = 1$). If the GIC increases, then the method propagates by replacing the k th support set element with its neighbor, i.e. the element in (53) that maximizes the GIC. Otherwise, the k th element stays in the estimated support. It is noted that if the GFOC method input is infeasible, i.e. $|\hat{\Omega}| > s$, then the input can be corrected by selecting the indices associated with the s largest values in $\hat{\mathbf{x}}$ where $\hat{\mathbf{x}} = (\mathbf{H}_{\hat{\Omega}}^T \mathbf{H}_{\hat{\Omega}})^{-1} \mathbf{H}_{\hat{\Omega}}^T \mathbf{y}$. The GFOC method is summarized in Algorithm 4. In addition, the following example illustrates the process of the GFOC method for a 9-node graph.

Example 1. Fig. 3 illustrates the following scenario: the GFOC method receives as input a set of measurements \mathbf{y} , a graph filter \mathbf{H} , and an estimated support set $\hat{\Omega} = \{3, 7\}$. The GFOC method starts by examining the first-order neighborhood of node 3 (the orange area). Specifically, it finds k such that $\{k, 7\}$ is the optimal support set that maximizes the GIC cost function in (18) within the sets: $\{3, 7\}$, $\{1, 7\}$, $\{4, 7\}$, and $\{6, 7\}$. Similarly, it examines the first-order neighborhood of node 7 (the green area). Hence, it finds m such that $\{k, m\}$ is the optimal support set that maximizes the GIC cost function in (18) within the sets $\{k, 7\}$, $\{k, 4\}$, $\{k, 5\}$, and $\{k, 9\}$.

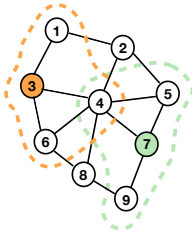


Figure 3: 9-node graph illustration: the one-hop neighborhoods of nodes 3 and 7, include the nodes inside the orange and green areas, respectively.

B. Discussion

The GFOC method is derived based on the GIC in (18) and the analysis in Section III, derived following Assumptions

Algorithm 4: GFOC

Input: Measurements \mathbf{y} , estimated support set $\hat{\Omega}$, graph $\mathcal{G}(\mathcal{V}, \mathcal{E})$, and graph filter \mathbf{H}

- 1 Define $obj(\Omega) = \|\mathbf{P}_{\mathbf{H}_{\Omega}} \mathbf{y}\|^2 - \rho|\Omega|$
- 2 Set $\hat{\Omega}^c = \hat{\Omega}$
- 3 **for** $k \in \hat{\Omega}$ **do**
- 4 Compute $\hat{m} = \arg \max_{m \in \mathcal{N}(k)} obj(\{\hat{\Omega}^c \setminus k\} \cup m)$
- 5 **if** $obj(\{\hat{\Omega}^c \setminus k\} \cup \hat{m}) > obj(\hat{\Omega}^c)$ **then**
- 6 $\Omega^c = \{\{\hat{\Omega}^c \setminus k\} \cup \hat{m}\}$
- 7 **end**
- 8 **end**
- 9 **Return** corrected support: Ω^c

A.1-A.2. Specifically, based on the discussion around (31), it can be inferred that when estimating the support set, if some errors occur, they are likely to be caused by the accidental inclusion of nodes in close proximity to the elements in the true signal support set Ω_t . These mistakenly included nodes may be in addition to, or instead of, some of the elements in Ω_t . In response to this possible error, Algorithm 4 proposes examining the immediate neighborhood of elements within the estimated support set to potentially enhance solutions w.r.t. the GIC. It is noted that using the GFOC method may only improve the performance compared to the method's input w.r.t. to the GIC. Moreover, it can be verified from Algorithm 4 that the number of GIC computations required is limited by $s d_{max}$, where d_{max} represents the maximum degree of the graph. Now, due to Assumption A.1, every node in the graph is connected to a small number of neighbors. Hence, we can assume that d_{max} is relatively low, i.e. $d_{max} \ll |\mathcal{V}|$. Thus, the computational complexity of this approach is expected to be low. It should be noted that the support of the output graph signal obtained by the GFOC method can be smaller than the input support set, as a single neighbor may replace two elements. The GFOC method can be easily extended to the graph Ψ order correction by replacing (53) with

$$\{\mathcal{N}_{\Psi}[k] \setminus k\} = \{m \in \mathcal{V} : 0 < \delta(k, m) \leq \Psi\}. \quad (54)$$

VI. SIMULATIONS

In this section, we evaluate the performance of the proposed support set recovery methods developed in Section IV and Section V, and compare them with existing methods through numerical simulations. The compared methods and the evaluation measures are presented in Subsection VI-A. We conduct three types of experiments to demonstrate the performance of our sparse recovery methods: 1) on synthetic data over random SBM graphs with known graph filters in Subsection VI-B; 2) for blind identification of graph signals over brain networks in Subsection VI-C; and 3) for recovering the source of the 1854 Cholera outbreak in London in Subsection VI-D.

A. Methods and Performance Measures

The following support set recovery methods are compared:

- The OMP method [31];

- The Lasso method [23], which is implemented for diffused sparse graph signals in [48];
- The BNB applied on (14) with the lower and upper bounds suggested in [65] for Boolean convex problems (denoted as ℓ_1 -BNB);
- The GM-GIC method in Algorithm 2;
- The Graph-BNB-GIC method in Algorithm 3 (denoted as G-BNB);
- An exhaustive search over the feasible set in (18) that involves comparing the cost functions of all the optional support sets (denoted as GIC);
- The GFOC support set correction method in Algorithm 4, with the estimated support set input from each of the above mentioned methods; The corrected outputs are denoted as 1) $\overline{\text{OMP}}^c$, 2) $\overline{\text{Lasso}}^c$, 3) $\overline{\ell_1 - \text{BNB}}^c$, 4) $\overline{\text{GM-GIC}}^c$, 5) $\overline{\text{G-BNB}}^c$, 6) $\overline{\text{GIC}}^c$.

In practice, the Lasso and ℓ_1 -BNB methods directly solve the sparse recovery problem in (14). As shown in Section II, this is equivalent to solving (16). The tuning factors for the different methods are stated as follows. The Lasso and ℓ_1 -BNB regularization parameter is set to 0.01. Additionally, the GIC penalty function, $\rho|\Omega|$, used for the GM-GIC, GIC, G-BNB, GIC, and GFOC methods, is chosen to be the AIC penalty function [64], which demonstrated efficacy across a variety of settings we evaluated. Hence, we set $\rho|\Omega| = 2|\Omega|$. For the GM-GIC method, the pre-screening threshold ζ in (37) is set to σ_n . For each presented scenario, the performance has been evaluated by at least 10^3 Monte Carlo simulations.

The following performance measures are used in the following to evaluate the different methods:

- The support set recovery is measured by the F-score classification metric [77]. The F-score compares between the true support set, Ω_t , and the estimated support, $\hat{\Omega}$, which is obtained by the different methods above. The F-score is given by

$$FS(\Omega_t, \hat{\Omega}) = \frac{2t_p}{2t_p + f_n + f_p}, \quad (55)$$

where $t_p \triangleq |\Omega_t \cap \hat{\Omega}|$ is the number of true-positives, $f_p \triangleq |\{\mathcal{V} \setminus \Omega_t\} \cap \hat{\Omega}|$ is the number of false-positives, and $f_n \triangleq |\Omega_t \cap \{\mathcal{V} \setminus \hat{\Omega}\}|$ is the number of false-negatives. The F-score is between 0 and 1, where 1 indicates perfect support set recovery, i.e. $\hat{\Omega} = \Omega$.

- The sparse signal recovery accuracy is measured using the MSE between the true graph signal, \mathbf{x} , and the estimated sparse graph signal, $\hat{\mathbf{x}}$: $MSE(\mathbf{x}, \hat{\mathbf{x}}) = \|\mathbf{x} - \hat{\mathbf{x}}\|_2^2$, where both \mathbf{x} and $\hat{\mathbf{x}}$ are normalized. In practice, the sparse signal is recovered by substituting $\hat{\Omega}$ in (15).
- The computational complexity is evaluated by the average run-time of the algorithms, where the simulations have been conducted using Matlab on two Intel(R) Xeon(R) CPU E5-2660 v4 @ 2.00 GHz processors (Subsection VI-B) or using Matlab on the Apple M1 pro chip (Subsections VI-C and VI-D).

B. Test Case A - Synthetic Data Set

In this subsection, we consider the support set recovery problem in (16), where the sparse dictionary matrix is selected as the graph filter defined by (6). The GSO used to construct the graph filter is the graph Laplacian matrix [3], i.e. $\mathbf{S} = \mathbf{L}$, which is normalized such that its largest eigenvalue is 12. The graph filter coefficients are set to 1, $h_j = 1$, $j = 0, \dots, \Psi$. Additionally, the measurement vector \mathbf{y} follows the model in (11). The underlying graph is modeled as an SBM graph with K clusters, where each cluster contains $N = 70$ nodes [78]. The probability of connection between any two nodes within the same cluster is $\frac{6}{N}$. In addition, consecutive clusters are connected by 2 link nodes from each cluster. Unless stated otherwise, in the following simulations the SBM is composed of 2 clusters and the support set elements in Ω , where $|\Omega| = 4$, are selected from one cluster using one of the following two cases:

- **Scenario 1 (Mixed Dispersed-Localized Support):** In this scenario, two nodes are randomly selected from the cluster, each has one of its neighbors added to the support set. This process is repeated until four different nodes are selected, which results in two groups of four distinct nodes. This scenario describes a situation where the non-zero elements are clustered in two separated groups, where the nodes within each group are in close proximity.
- **Scenario 2 (Localized Support):** In this scenario, a single node is randomly selected from the cluster. Then, $|\Omega| - 1$ (3 when $|\Omega| = 4$) of the node's neighbors are randomly chosen and added to the support set. This scenario describes a situation where the non-zero elements are in close proximity.

The non-zero elements of the sparse graph signal, \mathbf{x} , are drawn from a standard normal distribution. The filtered signal, $\mathbf{H}\mathbf{x}$, is normalized to a specified SNR, which is calculated as $\text{SNR} = \frac{\|\mathbf{H}\mathbf{x}\|^2}{(|\mathcal{V}|\sigma_n^2)}$, where the noise covariance matrix is $\mathbf{R} = \sigma_n^2 \mathbf{I}$, and unless otherwise specified, $\sigma_n = 0.01$.

Figures 4.(a)-(c) present the F-score as a function of: (a) the graph filter degree for SNR= 17 [dB] and $|\mathcal{V}| = 140$; (b) SNR for $\Psi = 4$ and $|\mathcal{V}| = 140$; and (c) and graph size for $\Psi = 4$ and SNR=20 [dB]. Across all figures, the GM-GIC and its correction $\overline{\text{GM-GIC}}^c$ methods obtain the closest result to the GIC benchmark, showing the highest F-scores. Close behind is the $\overline{\text{G-BNB}}^c$ method, with results up to 0.1 better than the G-BNB method in Fig. 4.(a). The results also show that GFOC significantly enhances the ℓ_1 -BnB method across all experiments.

In Fig. 4.(a), it can be seen that the F-score of all methods decreases almost always as the graph filter degree increases. The $\overline{\text{OMP}}^c$ method shows similar results to the $\overline{\text{G-BNB}}^c$ method for the first 2 graph degrees, yet lower F-scores at the higher degrees. The Lasso and ℓ_1 -BNB methods and their corrections show competitive results only for the first 2 graph degrees. In Fig. 4.(b) it can be seen that the F-score of all methods increases as the SNR increases. The corrected version of the OMP method, $\overline{\text{OMP}}^c$, improves the OMP F-score by approximately 25% compared to the original OMP. Similarly, the corrected version of the ℓ_1 -BNB, $\overline{\ell_1 - \text{BNB}}^c$ method, improves the F-score of the ℓ_1 -BNB by up to 20%. However,

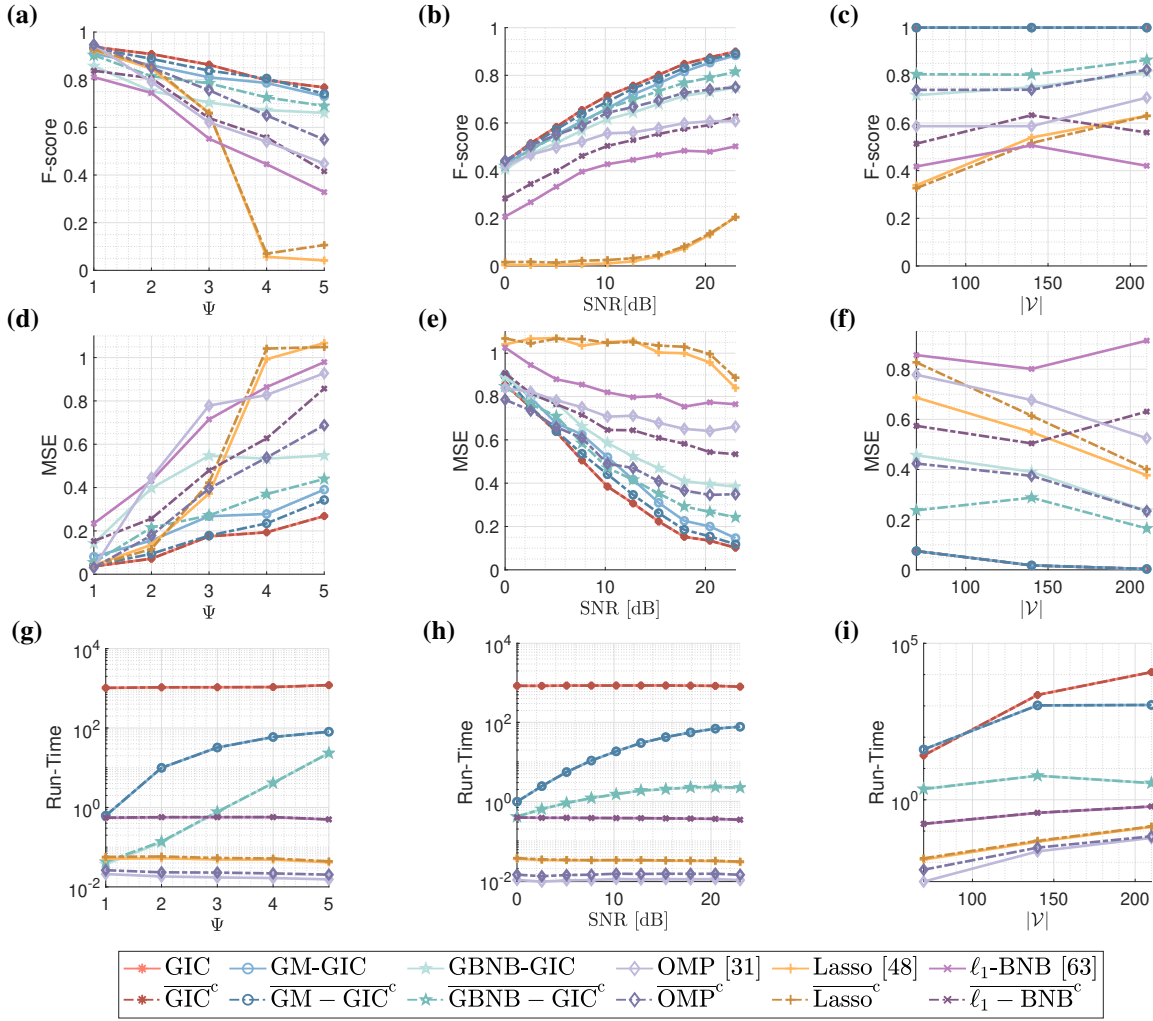


Figure 4: SBM graph model: The F-score ((a)-(c)), MSE ((d)-(f)), and run-time ((g)-(i)) of the different methods are compared versus the graph filter degree (Ψ), SNR, and graph size.

it remains less competitive than the $\overline{\text{OMP}}^c$, $\overline{\text{G-BNB}}^c$, and GM-GIC methods. The Lasso method and its corrected version exhibit poor F-score performance across all observed SNRs.

Figure 4.(c) displays the F-score as a function of graph size (number of SBM clusters). For $|V| = 70$, the graph contains one cluster. When $|V| = 140$, it has two clusters, with the signal support drawn from Cluster 1. For $|V| = 210$, the graph has three clusters, with the support either entirely from Cluster 1 or uniformly from Clusters 1 and 3. In all cases, the support follows Scenario 2, and the SNR is set to SNR=20 dB. It can be seen that the graph size has a minimal impact on the F-score of the proposed methods. The main effect is seen with the ℓ_1 and Lasso methods (and their corrections), which perform worse compared to the other approaches.

Figures 4.(d)-(f) presents the MSEs of the different methods as a function of the (a) graph filter degree, (b) the SNR, and (c) the graph size, using the same settings as those used for the F-score evaluation in Figs. 4.(a)-(c). The MSE performance in Figs. 4.(d)-(f) aligns closely with the F-scores results in Figs. 4.(a)-(c), leading to similar conclusions regarding the comparative performance of the different methods and the superiority of the proposed methods. For example, the GIC,

GM-GIC, and $\overline{\text{G-BNB}}^c$ methods, which achieve the highest F-scores in Figs. 4.(a)-(c), also exhibit the lowest MSEs in Figs. 4.(d)-(f). In addition, it can be seen in Fig. 4.(e) that the SNR significantly impacts the performance of the GIC, GM-GIC, and $\overline{\text{G-BNB}}^c$ methods, showing improvements of approximately 0.7 across the tested range. In contrast, the OMP method improves by only 0.1 and shows no further improvement beyond an SNR of 8 [dB]. Similarly, $\overline{\text{OMP}}^c$ improves by around 0.4 and shows no further improvement beyond an SNR of 14 [dB].

In Figs. 4.(g)-(i) we present the run-time of the different methods as a function of the (g) graph filter degree, (h) the SNR, (i) and the graph size, respectively, for the same setting as used for the F-score and MSE evaluation in Figs. 4.(a)-(c) and Figs. 4.(d)-(f). Across all figures, the GIC benchmark method requires the highest run-time, exceeding 1,000 seconds per Monte-Carlo simulation when the graph size is greater than 140 nodes. In contrast, the proposed GM-GIC and G-BNB methods have significantly reduced run-times while still maintaining good F-scores and MSE results, as shown in Figs. 4.(a)-(c) and Figs. 4.(d)-(f). The ℓ_1 -BNB, Lasso, and OMP methods are the fastest overall. However, as shown in

Figs. 4.(a)-(c) and Figs. 4.(d)-(f), these methods display lower F-scores and MSE, respectively, than the proposed methods. Notably, the additional run-time required by the GFOC method to correct these methods is negligible.

In Fig. 4.(g) it can be seen that the run-time of the GM-GIC and G-BNB methods increases as the graph filter degree increases, where the GM-GIC method run-time is larger than the G-BNB method run-time. In Fig. 4.(h), it can be seen that the run-time of the GM-GIC method significantly increases as the SNR increases. The run-time of the G-BNB method moderately increases and does not change for SNR higher than 15 [dB]. Both methods still operate significantly faster than the GIC method. The run-time required for the remaining methods is constant w.r.t. the SNR and lower than the methods mentioned above. In Fig. 4.(i) it can be seen that the run-time required for the GIC method grows exponentially with the graph (model) size. In comparison, the GM-GIC run-time grows significantly between $|\mathcal{V}| = 70$ to $|\mathcal{V}| = 140$, but remains constant between $|\mathcal{V}| = 140$ to $|\mathcal{V}| = 210$. The G-BNB method is only marginally affected by graph size. In addition, the graph size also affects the run-time of the Lasso and OMP methods, where their run-time becomes closer to those of the BNB methods as $|\mathcal{V}|$ increases. To conclude, the results demonstrate that the proposed GM-GIC and Graph-BNB-GIC scale well with the graph size and enable efficient processing even in larger network configurations.

C. Test Case B - Graph Blind Deconvolution of Brain Signals

Graph blind deconvolution has various real-world applications [48], [49]. In particular, it has been used for the analysis of epileptic seizures [79], [80] considered in this subsection. In this context, the graph signals are the neural activity levels in regions of interest (ROIs) within the brain, and the graph nodes and edges represent the brain regions and the anatomical connection between them, respectively. This application has been explored in GSP blind deconvolution studies [48], [49].

In order to apply our graph-based sparse recovery methods to the problem of blind deconvolution, we propose the following two-stage approach. In the first stage, a blind deconvolution is performed to estimate the unknown graph filter coefficients, \hat{h}_i , $i = 0, \dots, \Psi$, from the input measurements, \mathbf{y} . This estimation is implemented by one of the existing blind deconvolution methods, such as the methods in [48], [49]. The graph filter can then be recovered based on (6), where the GSO associated with the underlying graph is assumed to be known. Then, in the second stage, our graph-based sparse recovery methods are employed to reconstruct the sparse graph signal \mathbf{x} based on the model in (11), where the graph filter used is the one estimated in the previous stage. This overall two-stage approach is illustrated in Fig. 5.

In the following simulations, we consider the model in (11), where the graph filter is unknown and the underlying graph is a brain network. We use the Laplacian GSO, which is computed based on an adjacency matrix drawn from one of the six brain networks provided in [62], [81]. Entries in each row of the Laplacian that are significantly smaller (i.e. two orders of magnitude smaller than the maximum entry in the same row)

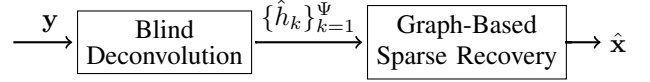


Figure 5: Two-stage approach for blind deconvolution combined with graph-based sparse recovery: The input measurements \mathbf{y} undergo a blind deconvolution process to estimate the graph filter coefficients, $\{\hat{h}_k\}_k, k = 1, \dots, \Psi$. Then, a graph-based sparse recovery is performed by the proposed methods, resulting in the estimated signal $\hat{\mathbf{x}}$.

are set to zero, and the Laplacian is subsequently normalized such that its largest eigenvalue is 12 to establish a controlled setting for the analysis.

The graph filter is constructed by setting the graph filter degree to $\Psi = 3$, substituting the Laplacian matrix and the graph filter coefficients (which are uniformly drawn from the interval $[0, 1]$) into (6), and normalizing the result to achieve a Frobenius norm of 1. The signal support is set to $\Omega = 4$ and is drawn according to Scenario 2 from Subsection VI-B. The non-zero values of the graph signals are uniformly drawn from the interval $[0, 1]$ and normalized to a unit-norm vector. This setup follows a similar framework to that considered in [49].

For the first stage of graph filter estimation, we use the following blind deconvolution techniques:

- **Blind Nuc. norm:** Employs nuclear norm minimization combined with ℓ_1 row sparsity regularization (see Equation (9) in [49]).
- **Blind Logdet:** Employs a log surrogate combined with ℓ_2 row sparsity regularization (see Equation (17) with $\tau_x = 0.5$ and $\tau_h = 0$ in [48]).

The performance of each scenario is evaluated through at least 300 Monte Carlo simulations.

We first evaluate the existence of Assumption A.1, which assumes a low maximal degree for the graph, in the context of the real-data brain networks. This assumption inherently indicates that the graph is sparse. Table I presents the ratio of the number of edges to the number of possible connections, $\frac{|\mathcal{E}|}{\frac{1}{2}|\mathcal{V}|(|\mathcal{V}|-1)}$, and the maximal degree, d_{\max} , for the six real-data brain networks derived from the dataset in [67]. as described above. This table demonstrates that these brain networks are sparse graphs with low maximal degrees, thus aligning with Assumption A.1.

	\mathcal{G}_1	\mathcal{G}_2	\mathcal{G}_3	\mathcal{G}_4	\mathcal{G}_5	\mathcal{G}_6
$\frac{ \mathcal{E} }{\frac{1}{2} \mathcal{V} (\mathcal{V} -1)}$	0.1	0.11	0.09	0.11	0.11	0.11
d_{\max}	3.28	4.41	5.83	3.87	3.93	3.68

Table I: Brain networks: the ratio of the number of edges and the number of possible connections, $\frac{|\mathcal{E}|}{|\mathcal{K}_n|}$, and the maximal degree, d_{\max} , for the real-data brain networks from [67], [81].

Next, we evaluate the graph-based methods from Subsection VI-A for three scenarios: 1) using a known graph filter; and 2) and 3) using the output of the two-stage blind deconvolution approach with the two different techniques, referred to as

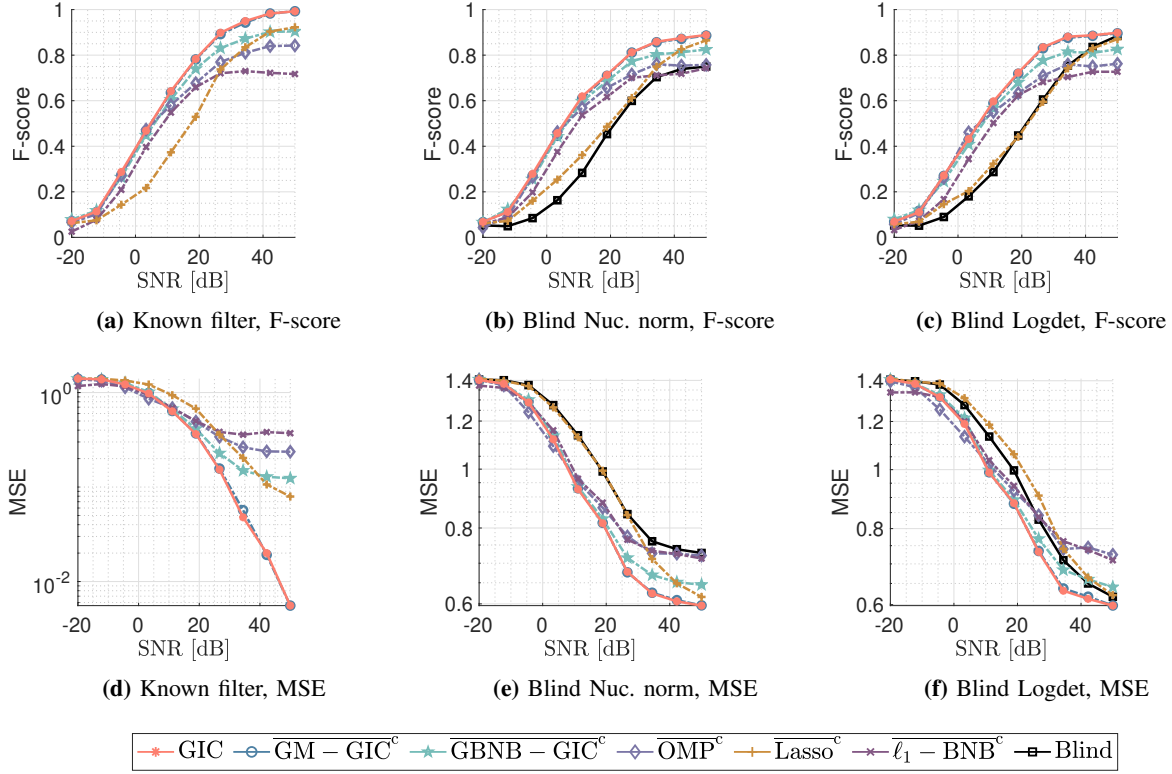


Figure 7: Brain networks: F-score and MSE of graph-based sparse recovery methods using graph coefficients that are either known (see (a) and (d)) or estimated via the blind deconvolution techniques: Blind Nuc. norm ((b) and (e)) and Blind Logdet ((c) and (f)).

“Blind Nuc. norm” and “Blind Logdet”, respectively. We compare the result of the different methods with those of the existing blind deconvolution methods, which can be interpreted as performing only Stage 1 of the approach described in Fig. 5. These methods are referred to as “Blind” in Fig. 7. In particular, in Figs. 5.(b) and 5.(e), the Blind Nuc. norm method is used, while in Figs. 5.(c) and 5.(f) the BLind Logdet method is employed. For the clarity of presentation, we only present the results for the graph-based methods after applying the GFOC method. This is because the GFOC method consistently improves the recovery performance with negligible additional computational overhead (run-time).

Figure 7 presents the F-score and MSE performance of the different methods as a function of the SNR. The MSE is computed as $MSE = \frac{1}{\|\mathbf{x}\mathbf{h}^T\|} \|\mathbf{x}\mathbf{h}^T - \hat{\mathbf{x}}\hat{\mathbf{h}}^T\|_F$, where \mathbf{x} is the sparse graph signal, $\hat{\mathbf{x}}$ is its estimator, \mathbf{h} represents the vector of graph filter coefficients, and $\hat{\mathbf{h}}$ is its estimator. For a known graph filter, we use $\hat{\mathbf{h}} = \mathbf{h}$.

Figures 7.(b)-(c) and 7.(e)-(f) show that the GIC, $\overline{\text{GM-GIC}}^c$, $\overline{\text{G-BNB}}^c$, and OMP^c methods significantly outperform the blind deconvolution techniques in both F-score and MSE under the case where the graph filter is unknown. These results confirm that the proposed sparse recovery methods are also applicable in scenarios where the graph filter is not known *a priori*. In addition, it can be seen in these figures that while OMP^c achieves competitive results at low SNR levels, its performance degrades as the SNR increases, and is worse than those of the $\overline{\text{GM-GIC}}^c$ and $\overline{\text{G-BNB}}^c$ methods. The Lasso^c , is

competitive to the above methods only at high SNR values, and the $\ell_1\text{-BnB}^c$ method works poorly for all SNR rates and even downgrades the blind deconvolution output. Notably, the F-scores of the graph-based sparse recovery methods, using the two-stage approach from Fig. 5, are comparable to those obtained where the graph filter is known, as can be seen by comparing the results in Figs. 7(a) with the results in Figs. 7.(b)-(c). In contrast, the MSE is more sensitive to the accuracy of the graph filter coefficients, indicating that improving the filter estimation could lead to better MSE results. It is also important to emphasize that the additional run-time for the $\overline{\text{G-BNB}}^c$, OMP^c , $\ell_1\text{-BnB}^c$, and Lasso^c methods have been found to be negligible compared to the computational cost of the first stage of the blind deconvolution. Thus, it is recommended that a subsequent graph sparse recovery stage be employed on the existing graph blind deconvolution methods.

D. Test Case C - Cholera Outbreak

In this section, we evaluate the performance of the different methods in a real-world test case where both the graph (network) and the graph filter are unknown. While the observation model in (11) forms the basis for our approach and underpins the proposed sparse recovery methods, it is important to note that in this scenario, the true structure of the real-world data and the underlying model are unknown. Thus, the simulations in this subsection demonstrate how the proposed framework can be applied to the practical application of interpreting real-

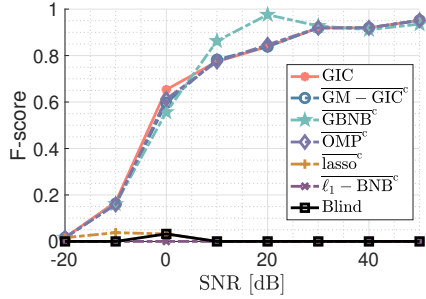


Figure 8: Cholera network: the F-score of graph-based sparse recovery methods using coefficients estimated via the Blind Nuc. norm method.

world data, despite the uncertainty in the true graph structure and graph filter that govern the system dynamics.

The real-world data for this case study, drawn from [68], involves the 1854 Cholera outbreak in London’s Soho district, where Dr. John Snow identified the source of the epidemic as a contaminated water pump [69]. Inspired by the framework in [40], this study applies the proposed graph-based sparse recovery methods to identify the source of the outbreak using historical data. The used dataset includes information on death tolls across 250 buildings, their geographic locations, and the positions of 8 water pumps, as provided in [68].

First, we model the underlying graph using a type-aware nearest neighbor structure. The graph is constructed based on the hypothesis that water was the primary transmission vector for cholera, with nodes representing buildings and pumps. For the graph edges, there is an edge between each pump and its two nearest pumps, each pump and its five nearest buildings, and each building and its two nearest buildings. The edge weights are computed using a Gaussian kernel:

$$W_{k,m} = \exp\left(-\frac{(\text{dist}(k,m))^2}{2 \cdot (f(k,m))^2}\right),$$

where dist represents the Euclidean distance, and $f(i,j)$ depends on the node types: $f(k,m) = 1000$ for pump connections, $f(k,m) = 80$ for pump-building connections, and $f(k,m) = 20$ for buildings connections. For ground truth, we consider the infected pump and the building with the highest death toll. To promote sparsity, we reduce the death count by one in each building, resulting in 136 non-zero elements out of 258, and we normalize the data vector to 1. It should be noted that the underlying graph and the graph filter are set to satisfy Assumptions A.1-A.2. Using the reconstructed graph, we apply the methodology outlined in Fig. 5, which includes a blind deconvolution step followed by graph-based sparse recovery. This follows the approach detailed in Subsection VI-C, with the estimated graph. Accordingly, we use the same methods as those described in Subsection VI-C, but with the estimated graph structure. The performance is evaluated using at least 60 Monte Carlo simulations.

Figure 8 shows the F-scores of the graph-based sparse recovery methods: GIC, GM-GIC^c, G-BNB^c, OMP^c, ℓ_1 -BNB^c, and Lasso^c, as a function of SNR. In each simulation, we added a zero-mean Gaussian additive noise to the data vector

to obtain the specific SNR. This evaluation focuses on the challenge of identifying the ground truth provided by the data vector contaminated with noise under different SNRs. The results indicate that the blind deconvolution method Blind Nuc. norm [49] cannot reconstruct the support set at any SNR level in this case. In contrast, the GIC, GM-GIC^c, G-BNB^c, and OMP^c methods have a significantly higher F-score and achieve close to perfect reconstruction (F-score > 0.9) for large SNR. These methods achieve similar F-scores for most SNRs, where the F-score increases as the SNR increases. Between 15 [dB] and 25 [dB], G-BNB^c achieves slightly higher results. Thus, the results in Fig. 8 demonstrate that the proposed graph-based sparse recovery methods offer substantial improvements in support set recovery, even in challenging real-world scenarios with unknown graph structures and filters, outperforming the existing blind deconvolution techniques. Notably, the run-time added by the graph-based methods, excluding the GIC method, is negligible in comparison to the run-time of the blind deconvolution method.

VII. CONCLUSIONS

In this paper, we propose three sparse recovery techniques: the GM-GIC, Graph-BNB-GIC, and GFOC methods. These techniques solve the support set recovery problem for diffused sparse graph signals, which are node-domain sparse graph signals diffused over the graph by a graph filter. The proposed methods use the GIC as the optimization cost function and leverage the underlying graphical structure to reduce the computational complexity and enhance the recovery performance. In particular, the GM-GIC and Graph-BNB-GIC directly tackle the support set recovery problem by considering local graph properties and efficiently partitioning the dictionary elements and iteratively searching over candidate support sets, respectively. The GFOC method is based on correcting the solution obtained by any other support set recovery technique. Furthermore, we provide a theoretical analysis of the considered setting with: 1) an examination of the dictionary matrix atoms (i.e. graph filter columns) derived from the underlying graphical structure; and 2) an evaluation of the computational complexity of the proposed methods, based on the graph filter degree, the maximum degree of the graph, and sparsity restrictions.

Simulations conducted over the SBM graphs reveal that the proposed GM-GIC and Graph-BNB-GIC methods achieve higher support set recovery and signal recovery accuracy compared to state-of-the-art methods such as OMP, Lasso, and ℓ_1 -BNB, while maintaining significantly lower computational overhead than the optimal GIC method. In general, the GM-GIC method outperforms the Graph-BNB-GIC method in terms of the accuracy of the support set recovery, but requires more computing time. It is also demonstrated that the GFOC method can significantly improve the support set recovery accuracy of existing methods, including the OMP, Lasso, and ℓ_1 -BNB methods, without imposing significant additional computation overhead. By applying the GFOC method on the Graph-BNB-GIC method, we obtained support set estimation results comparable to the GIC benchmark,

with a run-time comparable to the OMP and Lasso methods. Consequently, the best performance is obtained by combining the Graph-BNB-GIC and GFOC methods. In addition, we show the application of these methods for the problem of blind deconvolution in which the graph signal and the graph filter are unknown. Simulations conducted on brain networks and real data on the Cholera 1854 outbreak show that applying the proposed methods significantly improves the signal recovery performance for the application of blind deconvolution.

REFERENCES

- [1] G. Morgenstern and T. Routtenberg, "Sparse graph signal recovery by the graph-based multiple generalized information criterion (GM-GIC)," in *International Workshop on Computational Advances in Multi-Sensor Adaptive Processing (CAMSAP)*, 2023, pp. 491–495.
- [2] A. Ortega, P. Frossard, J. Kovačević, J. M. Moura, and P. Vanderghenst, "Graph signal processing: Overview, challenges, and applications," *Proc. IEEE*, vol. 106, no. 5, pp. 808–828, 2018.
- [3] D. I. Shuman, S. K. Narang, P. Frossard, A. Ortega, and P. Vanderghenst, "The emerging field of signal processing on graphs: Extending high-dimensional data analysis to networks and other irregular domains," *IEEE Signal Process. Mag.*, vol. 30, no. 3, pp. 83–98, 2013.
- [4] A. Sandryhaila and J. M. Moura, "Discrete signal processing on graphs," *IEEE Trans. Signal Process.*, vol. 61, no. 7, pp. 1644–1656, 2013.
- [5] —, "Discrete signal processing on graphs: Frequency analysis," *IEEE Trans. Signal Process.*, vol. 62, no. 12, pp. 3042–3054, 2014.
- [6] A. G. Marques, S. Segarra, G. Leus, and A. Ribeiro, "Stationary graph processes and spectral estimation," *IEEE Trans. Signal Process.*, vol. 65, no. 22, pp. 5911–5926, 2017.
- [7] E. Drayer and T. Routtenberg, "Detection of false data injection attacks in smart grids based on graph signal processing," *IEEE Syst. J.*, vol. 14, no. 2, pp. 1886–1896, 2019.
- [8] Y. Tanaka, Y. C. Eldar, A. Ortega, and G. Cheung, "Sampling signals on graphs: From theory to applications," *IEEE Signal Process. Mag.*, vol. 37, no. 6, pp. 14–30, 2020.
- [9] A. G. Marques, S. Segarra, G. Leus, and A. Ribeiro, "Sampling of graph signals with successive local aggregations," *IEEE Trans. Signal Process.*, vol. 64, no. 7, pp. 1832–1843, 2015.
- [10] S. Chen, A. Sandryhaila, J. M. Moura, and J. Kovačević, "Signal recovery on graphs: Variation minimization," *IEEE Trans. Signal Process.*, vol. 63, no. 17, pp. 4609–4624, 2015.
- [11] P. Di Lorenzo, P. Banelli, E. Isufi, S. Barbarossa, and G. Leus, "Adaptive graph signal processing: Algorithms and optimal sampling strategies," *IEEE Trans. Signal Process.*, vol. 66, no. 13, pp. 3584–3598, 2018.
- [12] G. Sagi and T. Routtenberg, "MAP estimation of graph signals," *IEEE Trans. Signal Process.*, vol. 72, pp. 463–479, 2024.
- [13] A. Kroizer, T. Routtenberg, and Y. C. Eldar, "Bayesian estimation of graph signals," *IEEE Trans. Signal Process.*, vol. 70, pp. 2207–2223, 2022.
- [14] A. Amar and T. Routtenberg, "Widely-linear mmse estimation of complex-valued graph signals," *IEEE Trans. Signal Process.*, vol. 71, pp. 1770–1785, 2023.
- [15] L. Dabush and T. Routtenberg, "Verifying the smoothness of graph signals: A graph signal processing approach," arXiv preprint: 2307.03210, 2023.
- [16] A. Venkitaraman, S. Chatterjee, and P. Händel, "Predicting graph signals using kernel regression where the input signal is agnostic to a graph," *IEEE Trans. Signal Inf. Process. Netw.*, vol. 5, no. 4, pp. 698–710, 2019.
- [17] E. Isufi, A. Loukas, A. Simonetto, and G. Leus, "Autoregressive moving average graph filtering," *IEEE Trans. Signal Process.*, vol. 65, no. 2, pp. 274–288, 2016.
- [18] M. Coutino, E. Isufi, and G. Leus, "Advances in distributed graph filtering," *IEEE Trans. Signal Process.*, vol. 67, no. 9, pp. 2320–2333, 2019.
- [19] S. S. Chen, D. L. Donoho, and M. A. Saunders, "Atomic decomposition by basis pursuit," *SIAM Review*, vol. 43, no. 1, pp. 129–159, 2001.
- [20] J. A. Tropp, "Greed is good: algorithmic results for sparse approximation," *IEEE Trans. Inf. Theory*, vol. 50, no. 10, pp. 2231–2242, Oct. 2004.
- [21] D. L. Donoho, M. Elad, and V. N. Temlyakov, "Stable recovery of sparse overcomplete representations in the presence of noise," *IEEE Trans. Inf. Theory*, vol. 52, no. 1, pp. 6–18, 2005.
- [22] M. Elad, *Sparse and Redundant Representations: From Theory to Applications in Signal and Image Processing*. New York, NY, USA: Springer Science & Business Media, 2010.
- [23] R. Tibshirani, "Regression shrinkage and selection via the lasso," *Journal of the Royal Statistical Society Series B: Statistical Methodology*, vol. 58, no. 1, pp. 267–288, 1996.
- [24] B. Efron, T. Hastie, I. Johnstone, and R. Tibshirani, "Least angle regression," *The Annals of Statistics*, vol. 32, no. 2, pp. 407–499, 2004.
- [25] E. Candes and T. Tao, "The dantzig selector: Statistical estimation when p is much larger than n," *The Annals of Statistics*, vol. 35, no. 6, pp. 2313–2351, 2007.
- [26] D. L. Donoho, A. Maleki, and A. Montanari, "Message-passing algorithms for compressed sensing," *Proceedings of the National Academy of Sciences*, vol. 106, no. 45, pp. 18914–18919, 2009.
- [27] D. P. Wipf and B. D. Rao, "Sparse bayesian learning for basis selection," *IEEE Trans. Signal Process.*, vol. 52, no. 8, pp. 2153–2164, 2004.
- [28] I. F. Gorodnitsky and B. D. Rao, "Sparse signal reconstruction from limited data using focuss: A re-weighted minimum norm algorithm," *IEEE Trans. Signal Process.*, vol. 45, no. 3, pp. 600–616, 1997.
- [29] R. Chartrand and W. Yin, "Iteratively reweighted algorithms for compressive sensing," in *ICASSP*, 2008, pp. 3869–3872.
- [30] S. G. Mallat and Z. Zhang, "Matching pursuits with time-frequency dictionaries," *IEEE Trans. Signal Process.*, vol. 41, no. 12, pp. 3397–3415, 1993.
- [31] T. T. Cai and L. Wang, "Orthogonal matching pursuit for sparse signal recovery with noise," *IEEE Trans. Inf. Theory*, vol. 57, no. 7, pp. 4680–4688, 2011.
- [32] W. Dai and O. Milenkovic, "Subspace pursuit for compressive sensing signal reconstruction," *IEEE Trans. Inf. Theory*, vol. 55, no. 5, pp. 2230–2249, 2009.
- [33] T. Blumensath and M. E. Davies, "Gradient pursuits," *IEEE Trans. Signal Process.*, vol. 56, no. 6, pp. 2370–2382, 2008.
- [34] J. Haupt, W. U. Bajwa, M. Rabbat, and R. Nowak, "Compressed sensing for networked data," *IEEE Signal Process. Mag.*, vol. 25, no. 2, pp. 92–101, 2008.
- [35] W. Xu, E. Mallada, and A. Tang, "Compressive sensing over graphs," in *2011 Proceedings IEEE INFOCOM*. IEEE, 2011, pp. 2087–2095.
- [36] M. Cheraghchi, A. Karbasi, S. Mohajer, and V. Saligrama, "Graph-constrained group testing," *IEEE Trans. Inf. Theory*, vol. 58, no. 1, pp. 248–262, 2012.
- [37] P. C. Pinto, P. Thiran, and M. Vetterli, "Locating the source of diffusion in large-scale networks," *Physical review letters*, vol. 109, no. 6, p. 068702, 2012.
- [38] E. Sefer and C. Kingsford, "Diffusion archeology for diffusion progression history reconstruction," *Knowledge and information systems*, vol. 49, pp. 403–427, 2016.
- [39] P. Zhang, J. He, G. Long, G. Huang, and C. Zhang, "Towards anomalous diffusion sources detection in a large network," *ACM Transactions on Internet Technology (TOIT)*, vol. 16, no. 1, pp. 1–24, 2016.
- [40] R. Pena, X. Bresson, and P. Vanderghenst, "Source localization on graphs via ℓ_1 recovery and spectral graph theory," in *Image, Video, and Multidimensional Signal Processing Workshop (IVMSP)*, 2016, pp. 1–5.
- [41] A. Sridhar, T. Routtenberg, and H. V. Poor, "Quickest inference of susceptible-infected cascades in sparse networks," in *International Symposium on Information Theory (ISIT)*, 2023, pp. 102–107.
- [42] X. Wang, P. Liu, and Y. Gu, "Local-set-based graph signal reconstruction," *IEEE Trans. Signal Process.*, vol. 63, no. 9, pp. 2432–2444, 2015.
- [43] A. Anis, A. Gadde, and A. Ortega, "Towards a sampling theorem for signals on arbitrary graphs," in *ICASSP*, 2014, pp. 3864–3868.
- [44] S. Chen, R. Varma, A. Sandryhaila, and J. Kovacevic, "Discrete signal processing on graphs: Sampling theory," *IEEE Trans. Signal Process.*, vol. 63, no. 24, pp. 6510–6523, 2015.
- [45] M. Tsitsvero, S. Barbarossa, and P. Di Lorenzo, "Signals on graphs: Uncertainty principle and sampling," *IEEE Trans. Signal Process.*, vol. 64, no. 18, pp. 4845–4860, 2016.
- [46] M. B. Mashhadi, M. Fallah, and F. Marvasti, "Interpolation of sparse graph signals by sequential adaptive thresholds," in *2017 International Conference on Sampling Theory and Applications (SampTA)*. IEEE, 2017, pp. 266–270.
- [47] D. Romero, M. Ma, and G. B. Giannakis, "Kernel-based reconstruction of graph signals," *IEEE Transactions on Signal Processing*, vol. 65, no. 3, pp. 764–778, 2016.
- [48] D. Ramírez, A. G. Marques, and S. Segarra, "Graph-signal reconstruction and blind deconvolution for structured inputs," *Signal Process.*, vol. 188, p. 108180, 2021.

- [49] S. Segarra, G. Mateos, A. G. Marques, and A. Ribeiro, "Blind identification of graph filters," *IEEE Trans. Signal Process.*, vol. 65, no. 5, pp. 1146–1159, 2016.
- [50] S. Segarra, A. G. Marques, and A. Ribeiro, "Optimal graph-filter design and applications to distributed linear network operators," *IEEE Trans. Signal Process.*, vol. 65, no. 15, pp. 4117–4131, 2017.
- [51] —, "Distributed implementation of linear network operators using graph filters," in *Annual Allerton Conference on Communication, Control, and Computing (Allerton)*, 2015, pp. 1406–1413.
- [52] J. Mei and J. M. Moura, "Signal processing on graphs: Estimating the structure of a graph," in *ICASSP*, 2015, pp. 5495–5499.
- [53] H. Rainer and U. Krause, "Opinion dynamics and bounded confidence: Models, analysis and simulation," *Journal of Artificial Societies and Social Simulation*, vol. 5, no. 3, 2002.
- [54] D. Shah and T. Zaman, "Rumors in a network: Who's the culprit?" *IEEE Trans. Inf. Theory*, vol. 57, no. 8, pp. 5163–5181, 2011.
- [55] M. E. Newman, "Spread of epidemic disease on networks," *Physical review E*, vol. 66, no. 1, p. 016128, 2002.
- [56] D. Shah and T. Zaman, "Detecting sources of computer viruses in networks: theory and experiment," in *Proceedings of the ACM SIGMETRICS international conference on Measurement and modeling of computer systems*, 2010, pp. 203–214.
- [57] G. Morgenstern and T. Routtenberg, "Structural-constrained methods for the identification of unobservable false data injection attacks in power systems," *IEEE Access*, vol. 10, pp. 94 169–94 185, 2022.
- [58] G. Morgenstern, J. Kim, J. Anderson, G. Zussman, and T. Routtenberg, "Protection against graph-based false data injection attacks on power systems," *IEEE Trans. Control Netw. Syst.*, pp. 1–12, 2024.
- [59] S. Segarra, A. G. Marques, G. Leus, and A. Ribeiro, "Reconstruction of graph signals through percolation from seeding nodes," *IEEE Trans. Signal Process.*, vol. 64, no. 16, pp. 4363–4378, 2016.
- [60] Y. Zhu, F. J. I. Garcia, A. G. Marques, and S. Segarra, "Estimating network processes via blind identification of multiple graph filters," *IEEE Trans. Signal Process.*, vol. 68, pp. 3049–3063, 2020.
- [61] C. Ye, R. Shafipour, and G. Mateos, "Blind identification of invertible graph filters with multiple sparse inputs," in *European Signal Processing Conference (EUSIPCO)*, 2018, pp. 121–125.
- [62] F. J. Iglesias, S. Segarra, S. Rey-Escudero, A. G. Marques, and D. Ramirez, "Demixing and blind deconvolution of graph-diffused sparse signals," in *ICASSP*, 2018, pp. 4189–4193.
- [63] S. Rey-Escudero, F. J. I. Garcia, C. Cabrera, and A. G. Marques, "Sampling and reconstruction of diffused sparse graph signals from successive local aggregations," *IEEE Signal Process. Lett.*, vol. 26, no. 8, pp. 1142–1146, 2019.
- [64] P. Stoica and Y. Selen, "Model-order selection: a review of information criterion rules," *IEEE Signal Process. Mag.*, vol. 21, no. 4, pp. 36–47, 2004.
- [65] S. Boyd and J. Mattingley, "Branch and bound methods," *Notes for EE364b, Stanford University*, vol. 2006, p. 07, 2007.
- [66] E. L. Lawler and D. E. Wood, "Branch-and-bound methods: A survey," *Operations research*, vol. 14, no. 4, pp. 699–719, 1966.
- [67] P. Hagmann, L. Cammoun, X. Gigandet, R. Meuli, C. J. Honey, V. J. Wedeen, and O. Sporns, "Mapping the structural core of human cerebral cortex," *PLoS biology*, vol. 6, no. 7, p. e159, 2008.
- [68] R. Wilson, "John Snow's famous Cholera analysis data in modern GIS formats," 2012.
- [69] J. Snow *et al.*, "Report on the cholera outbreak in the parish of st. james," *James, Westminster; during the Autumn of 1854*, pp. 97–120, July 1855.
- [70] Z. Wang, A. Scaglione, and R. J. Thomas, "Generating statistically correct random topologies for testing smart grid communication and control networks," *IEEE Trans. Smart Grid*, vol. 1, pp. 28–39, 2010.
- [71] S. M. Kay, *Fundamentals of statistical signal processing: Estimation Theory*. New Jersey, NJ, USA: Prentice Hall PTR, 1993, vol. 1.
- [72] H. Yanai, K. Takeuchi, and Y. Takane, "Projection matrices," in *Projection Matrices, Generalized Inverse Matrices, and Singular Value Decomposition*. Springer, 2011, pp. 25–54.
- [73] P. Babu and P. Stoica, "Multiple-hypothesis testing rules for high-dimensional model selection and sparse-parameter estimation," *Signal Process.*, vol. 213, p. 109189, 2023.
- [74] S. M. Kay, *Fundamentals of Statistical Signal Processing, Volume II: Detection Theory*. New Jersey, NJ, USA: Prentice Hall PTR, 1993.
- [75] R. Dionne and M. Florian, "Exact and approximate algorithms for optimal network design," *Networks*, vol. 9, no. 1, pp. 37–59, 1979.
- [76] R. S. Solanki, J. K. Gorti, and F. Southworth, "Using decomposition in large-scale highway network design with a quasi-optimization heuristic," *Transportation Research Part B: Methodological*, pp. 127–140, 1998.
- [77] M. Sokolova and G. Lapalme, "A systematic analysis of performance measures for classification tasks," *Information Processing and Management*, vol. 45, pp. 427–437, 07 2009.
- [78] C. Lee and D. J. Wilkinson, "A review of stochastic block models and extensions for graph clustering," *Applied Network Science*, vol. 4, no. 1, pp. 1–50, 2019.
- [79] M. A. Kramer, E. D. Kolaczyk, and H. E. Kirsch, "Emergent network topology at seizure onset in humans," *Epilepsy research*, vol. 79, no. 2-3, pp. 173–186, 2008.
- [80] P. Mathur and V. K. Chakka, "Graph signal processing of EEG signals for detection of epilepsy," in *SPIN*, 2020, pp. 839–843.
- [81] S. Iglesias, "Blind separation of sparse signals diffused on graphs," GitHub repository, [Online]. Available: https://github.com/figlesias/gsp_bss, 2018, accessed: 2024-09-26.